Nanostructure of biogenic *versus* abiogenic calcium carbonate crystals

JAROSŁAW STOLARSKI and MACIEJ MAZUR

Stolarski, J. and Mazur, M. 2005. Nanostructure of biogenic *versus* abiogenic calcium carbonate crystals. *Acta Palaeontologica Polonica* 50 (4): 847–865.

The mineral phase of the aragonite skeletal fibers of extant scleractinians (*Favia*, *Goniastrea*) examined with Atomic Force Microscope (AFM) consists entirely of grains ca. 50–100 nm in diameter separated from each other by spaces of a few nanometers. A similar pattern of nanograin arrangement was observed in basal calcite skeleton of extant calcareous sponges (*Petrobiona*) and aragonitic extant stylasterid coralla (*Adelopora*). Aragonite fibers of the fossil scleractinians: Neogene *Paracyathus* (Korytnica, Poland), Cretaceous *Rennensismilia* (Gosau, Austria), *Trochocyathus* (Black Hills, South Dakota, USA), Jurassic *Isastraea* (Ostromice, Poland), and unidentified Triassic tropiastraeid (Alpe di Specie, Italy) are also nanogranular, though boundaries between individual grains occasionally are not well resolved. On the other hand, in diagenetically altered coralla (fibrous skeleton beside aragonite bears distinct calcite signals) of the Triassic corals from Alakir Cay, Turkey (*Pachysolenia*), a typical nanogranular pattern is not recognizable. Also aragonite crystals produced synthetically in sterile environment did not exhibit a nanogranular pattern. Unexpectedly, nanograins were recognized in some crystals of sparry calcite regarded as abiotically precipitated. Our findings support the idea that nanogranular organization of calcium carbonate fibers is not, *per se,* evidence of their biogenic *versus* abiogenic origin or their aragonitic *versus* calcitic composition but rather, a feature of $CaCO_3$ formed in an aqueous solution in the presence of organic molecules that control nanograin formation. Consistent orientation of crystalographic axes of polycrystalline skeletal fibers in extant or fossil coralla, suggests that nanograins are monocrystalline and crystallographically ordered (at least after deposition). A distinctly granular *versus* an unresolvable pattern of nano-organization of $CaCO_3$ fibers seems to correspond, respectively, to an original *versus* a diagenetically depleted amount of organic matter bounding a mineral phase; this is consistent with qualitative and quantitative analyses of organic matter content in extant and fossil skeletons.

Key words: Scleractinia, Stylasteridae, Calcarea, biominerals, aragonite, calcite, nanostructure, AFM.

Jarosław Stolarski [stolacy@twarda.pan.pl], Instytut Paleobiologii, Polska Akademia Nauk, ul. Twarda 51/55, PL-00-818 Warszawa, Poland;
Maciej Mazur [mmazur@chem.uw.edu.pl], Wydział Chemii, Uniwersytet Warszawski, ul. Pasteura 1, PL-02-093 Warszawa, Poland.

Introduction

Invertebrate skeletons conventionally described as coralla, shells or tests, can be viewed as hierarchical constructions encompassing several structural levels. Most commonly, crystal-like fibers called also biocrystals (see Glossary) are considered the smallest units within the skeletal hierarchy; individual biocrystals are arranged into larger units (e.g., bundles or clusters of fibers), these may form layers, layers may contribute to the formation of still larger structures e.g., plates, opercula, etc., and finally, a group of diversely organized high level structures form the skeleton of the whole organism. Interestingly, remarkable diversity is often observed among the structures positioned just at the lower level of structural hierarchy (i.e., among fibers or their clusters). In many invertebrates (e.g., corals, mollusks), distinct patterns of skeleton microstructural organization appear to be a source of phylogenetically and taxonomically important information, complementary to macromorphological and molecular data. This aspect of in-depth skeletal studies—very promising from the paleontological perspective in showing the value of skeletal data—envokes interest in searching for a link between the biological (biochemical, genetically-driven) and physicochemical (geochemical, environmentally-controlled) constraints of skeleton formation at various structural levels. This can be attempted using different analytical instruments and procedures, including retrieval of diverse biogeochemical and isotopic signatures from the biocrystals and their further use as (paleo) environmental and/or (paleo)physiological ("vital effect") proxies (recent examples: Sinclair 2005 for corals; Geist et al. 2005 for mollusks).

An interesting aspect of the interplay between biological and physicochemical factors is the occurrence of organic components (organic matrix) embedded within the mineral phase of the skeleton (Towe 1972). During skeleton formation, these organic components (later intraskeletal) play an important and active role in regulation of the biomineralization process: i.e., delineate the space where mineralization takes place, regulate activity, nucleation and transportation of ions that participate in mineral formation, etc. (excellent overview in Mann 2001).

They become incorporated in the skeleton either because they are indispensable components by the very end of biomineralization process, or are occluded only because there is no mechanism for their removal from the mineralization site.

Until recently, it was commonly assumed that the skeletal fibers are purely inorganic crystals: e.g., aragonitic in scleractinian coralla, basal skeletons of coralline sponges and molluscan nacre layers, or calcitic in prismatic layer of many bivalves and stereome of echinoderms. Indeed, a crystalline, mineral phase was spatially separated from the organic one as shown by fluorescence microscope studies of "organic envelopes" of bundles of fibers or organic bands sandwiched between successive layers of fibers (e.g., Gautret et al. 2000; Stolarski 2003) or X-ray-Absorption Near Edge structure Spectroscopy (XANES) observations of S-sulfate components (Cuif et al. 2003). Indirectly, separation of two skeletal phases was also suggested by the etching techniques showing clear-cut (in SEM magnification range) selective etching of organic (enzymatic solutions) or, respectively, mineral phase components (acidic etching of mineral phase with glutaraldehyde fixation of the organic phase) (Cuif et al. 1997; Cuif and Sorauf 2001).

However, recent studies of calcium carbonate biocrystals reveal that the organic and mineral components are not separated in the microscale and that seemingly monocrystalline fibers are actually composed of densely packed grains, tens of nanometers in diameter, embedded in a thin layer of organic material (Dauphin 2001; Cuif et al. 2004; Cuif and Dauphin 2005a, b; Rousseau et al. 2005). This new paradigm of structural organization of calcareous biocrystals emerges due to the rapid introduction to the life-sciences of the most advanced instruments operating at the nanoscale: Field Emission Scanning Electron Microscope (FESEM; e.g., Clode and Marshall 2003a), Atomic Force Microscope (AFM; see references below), or high-resolution analytical tools like the NanoSIMS ion microprobe (e.g., Meibom et al. 2004). The most accurate morphological characterization of nanostructure is provided by the AFM[1]. Although, by default, the instrument allows one only to visualize the surface of examined material, special scanning operational modes, enabling detection of adhesion, friction (lateral force), viscoelasticity (phase imaging, force modulation) of the sample, as well as matched techniques of material preparation, allow one also to indirectly characterize physicochemical properties of the sample.

Studies on the nanostructure of invertebrate skeletons are still in the early phase of development, and with a few exceptions (e.g., Dauphin 2002) deal with extant materials. The question explored in this report is the assessment of nanostructural diagenetic effects on fossil aragonite biocrystals that are considered "excellently preserved" from a macro- and microstructural perspective. We focused mainly on aragonitic skeletons of scleractinian corals, in particular on the thickening fibers that contain more mineral than organic phase in comparison to the deposits of the Rapid Accretion Front "calcification centers" (Stolarski 2003). In our preliminary approach, we also tried to assess whether the occurrence of nanograins is an exclusive feature of biogenic calcium carbonate fibers or if they can also be recognized in calcareous structures formed without the direct control of a living organism.

Institutional abbreviations.—Specimens are housed in the following institutions: Dipartimento del Museo di Paleobiologia e dell'Orto Botanico, Università di Modena e Reggio Emilia, Modena, Italia (IPUM), Institute of Paleobiology, Polish Academy of Sciences, Warsaw (ZPAL), and National Museum of Natural History, Washington D.C. (USNM).

Other abbreviations.—AFM, Atomic Force Microscopy; (d)CRA, (deposits of) Centers of Rapid Accretion; EDS, Energy Dispersive Spectroscopy; FESEM, Field Emission Scanning Electron Microscopy; MFM, Molecular Fluorescence Microscopy; RAF, Rapid Accretion Front; SEM, Scanning Electron Microscopy; WDS, Wavelength Dispersive Spectroscopy; XRD, X-ray Diffraction.

Materials and methods

Recent and fossil samples.—Materials examined consisted mostly of scleractinian coralla, both extant (*Favia*, *Goniastraea*) and fossil (*Paracyathus*, *Rennensismilia*, *Trochocyathus*, *Isastraea*, *Pachysolenia*, and an undetermined tropidastraed); comparative skeletons included the basal, calcitic skeleton of an extant calcareous sponge (*Petrobiona*) and aragonitic stylasterid coenosteum (*Adelopora*). Fossil localities containing the well preserved scleractinian corals listed above are described in extensive literature: Korytnica, Holy Cross Mts., Poland (Neogene, Miocene), Stolarski (1991); Gosau, Austria (Santonian, Cretaceous), Felix (1903), Sorauf (1999); Dry Creek, Black Hills, South Dakota USA (Santonian–lower Maastrichtian, Cretaceous), Wells (1933); Ostromice, Northwest Poland (Oxfordian, Jurassic), Roniewicz (1982, 1984); Alpe di Specie, Dolomites, Italy (upper Carnian, Triassic), Volz (1896); Alakir Çay valley, Antalya, Turkey (lower Norian, Triassic), Cuif et al. (1972), Cuif (1975). Additional taxonomic and locality details are given in figure captions.

The main criterion of fossil materials selection was their good preservation state: specimens were initially selected under a stereoscopic microscope for the presence of features that most commonly occur in fossils with preserved original mineralogy (discernible bundles of fibers on broken or thin sections, light color of the skeleton, etc.); later the mineralogy of the sample was confirmed using Feigl's solution (stains the aragonite surface black, whereas the coexisting calcite remains unchanged in color; Friedman 1959), and XRD analysis. With

[1] AFM allows a magnitude higher magnification of the surface topography (up to 1,000,000X) in comparison to Scanning Electron Microscope (SEM, magnification as great as 100,000X), and thousands of magnitudes higher than traditional light microscope techniques (magnifications as great as 1000X).

the exception of lower Norian *Pachysolenia cylindrica* Cuif, 1975 whose skeleton was partly calcitized, the mineralogy of other coralla was aragonitic. Geochemical analyses of selected samples helped indirectly to assess diagenetic alteration of the skeleton. Distribution of minor elements (especially Sr, Mg) within skeleton and cements is used as a way of identifying organic aragonite (containing high Sr and low Mg contents), neomorphic calcite (containing high Mg and low Sr contents; Sorauf and Cuif 2001, see also discussion below under Nanotaphonomy). The same sample selection was also stained with acridine orange dye and examined under a fluorescence microscope (filter setting identical to Stolarski 2003: 498) to determine possible fluorescent response of organic components. In addition to this, thermal analysis of three coral samples (selected according to the obtained results of nanostructural observations) was performed using the thermogravimetric technique.

In addition to biogenic aragonitic samples, we also made a preliminary survey of various calcium carbonate crystals that conventionally are considered to have abiogenic origin. In this report we illustrate different nanostructures from two samples of sparry calcite cements that filled, in places, the interseptal space of coral from the upper Carnian (Triassic) deposits of Alpe di Specie, Italy, and respectively, upper Maastrichtian (Cretaceous) deposits of Lubycza Królewska, Poland (Cieśliński and Rzechowski 1993). Comparative samples of abiogenic calcites included: sparry calcite cements developed within brachipod and serpulid shells from the Upper Jurassic (lower Tithonian) deposits of Vršatec (Slovakia), as well as calcite crystals from Neogene (Pleistocene) karstic deposits of Działoszyn (Poland).

Equipment.—Recent and fossil samples were preliminarily selected using Nikon SMZ800 stereoscopic zoom microscope. Polished sections were examined using conventional transmitted light microscope (Olympus BX50) and MFM (Nikon Eclipse 80i) fitted with epi-fluorescence attachment and cooled camera head DS-5Mc. Micrographs were taken using a 494 nm excitation filter and 520 nm emission filter. Polished, non-etched and etched samples were investigated using SEM (Philips XL 20), AFM (Digital Instruments Nanoscope IIIa [Veeco]) microscopes. X-ray elemental mappings were acquired on a Cameca SX-100 electron microprobe using wavelength-dispersive techniques (WDS, the parameters are the same as used by Stolarski 2003: 499), whereas bulk elemental analyses using Energy Dispersive Spectroscopy (EDS) were performed on a Philips XL-20 scanning microscope coupled with the EDS detector ECON 6, system EDX-DX4i. Thermogravimetric measurements were made using Q 1500 D Derivatograph (Magyar Optikai Művek, Budapest).

Preparatory techniques.—Various preparatory techniques were chosen depending on the type of instrument used as described below.

AFM: The samples prepared for AFM should have a very low surface relief, typically not exceeding ca. 3.5 μm (preferable a few hundred nanometers); larger values would damage the tip of the device. This limitation determines the way of sample preparation: the section cannot be broken (this could instantly show heterogeneity of the material without further preparation) but polished and chemically prepared to emphasize structural and compositional diversity of the sample. All samples used in this study were fixed with araldite (Araldite 2020, a two component, room temperature curing, low viscosity adhesive transparent epoxy) and ground with diamond suspension having grain sizes of 5 and 1 micrometers, and later polished with aluminium oxide (Buehler TOPOL 3 final polishing suspension with particle size 0.25 micrometers). After polishing, sections were rinsed in Milli-Q water and washed in an ultrasonic cleaner for 10 seconds. Polished samples were etched selectively with respect to organic components using buffered oxidizing solution. Etching procedure encompassed immersion of the polished samples for 10 min in McIlvain buffer (pH = 8) containing 1% ammonium persulfate. Then, they were removed from the solution, rinsed with deionized water and dried.

MFM: For MFM observations, sections were stained in a 0.45 μm filtered 1% acridine orange aqueous solution for 5 minutes. Stained samples were briefly rinsed in distilled water and air dried.

SEM: Polished sections were etched for 10 seconds in 0.1% formic acid, then rinsed with Milli-Q water and air dried. After drying, the specimens were put on stubs with double sticky tape and sputter-coated with conductive platinum film.

Thermogravimetry: Powdered samples (400 mg) were heated in air environment under linear gradient (10°C min^{-1}) from ambient 20°C to 1000°C.

Synthetic aragonite.—Synthetic aragonite was precipitated inorganically at room temperature on glass slides from saturated aqueous solution of $CaCO_3$ containing magnesium chloride.

The saturated solution was prepared by slow addition of 100 ml of Na_2CO_3 (0.1M) into stirred 100 ml $CaCl_2$ (0.12 M) containing $MgCl_2$ (0.06 M). After precipitation of the salt, the $CaCO_3$ was allowed to accumulate at the bottom of the reaction vessel until the solution above the deposit was clear. This solution (being with contact with the precipitate) was used for further growing of aragonite on glass substrates.

The glass slides (Menzelglaser) were cut into 1cm × 1cm pieces and cleaned in piranha solution (3:1 v/v ratio of concentrated sulfuric acid and hydrogen peroxide) for 15 min. Then, the substrates were removed, rinsed with deionised water (MilliQ), dried and placed in saturated $CaCO_3$ solution for 2 or 7 days for growing of aragonite. The resulting deposits (precipitation time: 7 days) consisted of bundles of acicular fibers forming clusters ca. 80 mm in diameter as shown by SEM (Fig. 1A, B). Shortening the deposition time (2 days) resulted in formation of smaller aragonite crystals (Fig. 1C, D) that were more suitable for AFM imaging. The slides with $CaCO_3$ precipitate were subsequently removed from the solution, immediately rinsed with water and dried.

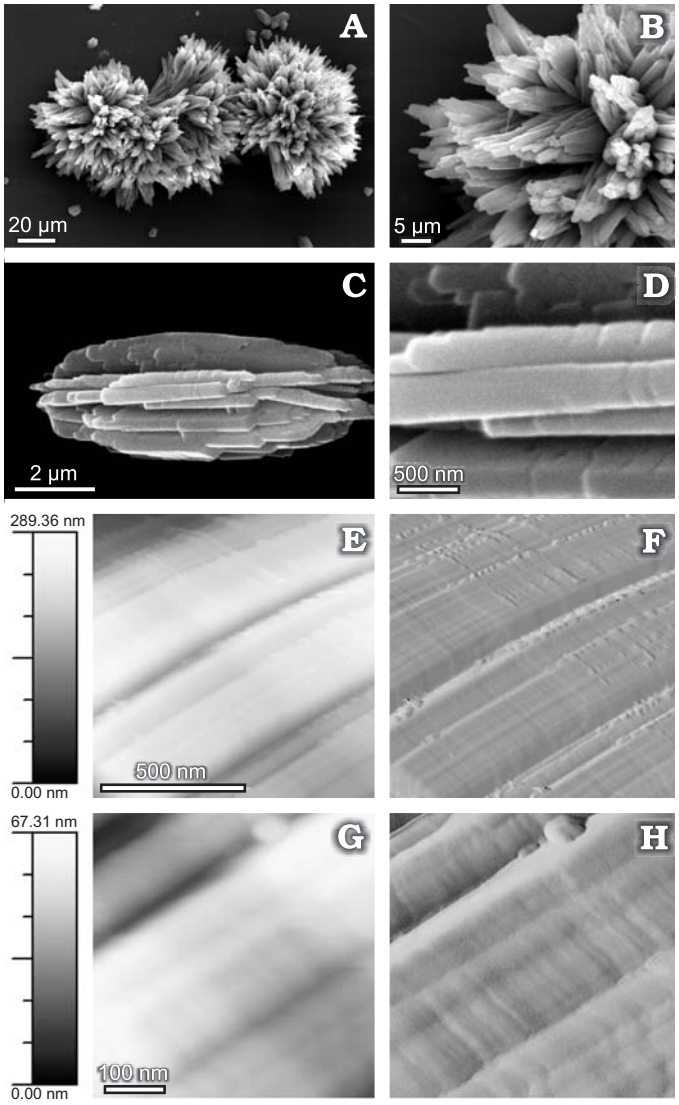

Fig. 1. Synthetic aragonite crystals. Seven day old cluster of acicular aragonite crystals, overall (**A**) and close-up (**B**) views. Two day old cluster of acicular aragonite (**C**) with growth steps (**D**). No distinct nanograins are recognizable on crystal surface before and after (E–H) treatment with oxidizing solution. AFM (contact mode; buffered pH = 8, ammonium persulfate 1%, 10 min.): height-2D projection (**E**, **G**), and deflection (**F**, **H**) images of 1×1 µm (E, F) and 500×500 nm (G, H) crystal face. Grayscale bars (left) show z-scale (height) of 2D projection images.

Chemicals.—Sodium carbonate (Sigma-Aldrich, 99.5+%), calcium chloride (Sigma-Aldrich, > 96%), magnesium chloride (POCh, reagent grade), ammonium persulfate (Fluka, > 98%), McIlvain buffer pH = 8 (Chempur), formic acid (POCh, 85%), acridine orange (Sigma-Aldrich, 90%).

Software.—AFM pictures in native Digital Instrument's Nanoscope file format were, for the final presentation, imported and processed using WsxM free software (downloadable at http://www.nanotec.es) and exported as high resolution TIFF images. Images recorded during sample examination using SEM, WDS, and MFM were recorded in native TIFF format. The thermogravimetrical (TG), differential thermogravimetrical (DTG), and differential thermo-analytical (DTA) curves were recorded using DERIVAT software (Medson Electronics; Poznań-Paczkowo, Poland). The composite figures were assembled from TIFF images imported to CorelDraw 11 graphics software.

Results

The starting point of the present study was to determine the nanostructure of synthetically produced crystals of aragonite, submitted to the same preparative procedures as the rest of the AFM-examined samples. A rationale was to check if chemical preparation (buffered oxidizing solution) does not produce nanostructural artefacts (see Discussion). Examining of nanostructures of calcareous skeleton of extant invertebrates was, in turn, a reference point for studies of fossil calcareous biocrystals. At the end, biocrystal nanostructures were compared with crystals of sparry calcite considered abiotically produced.

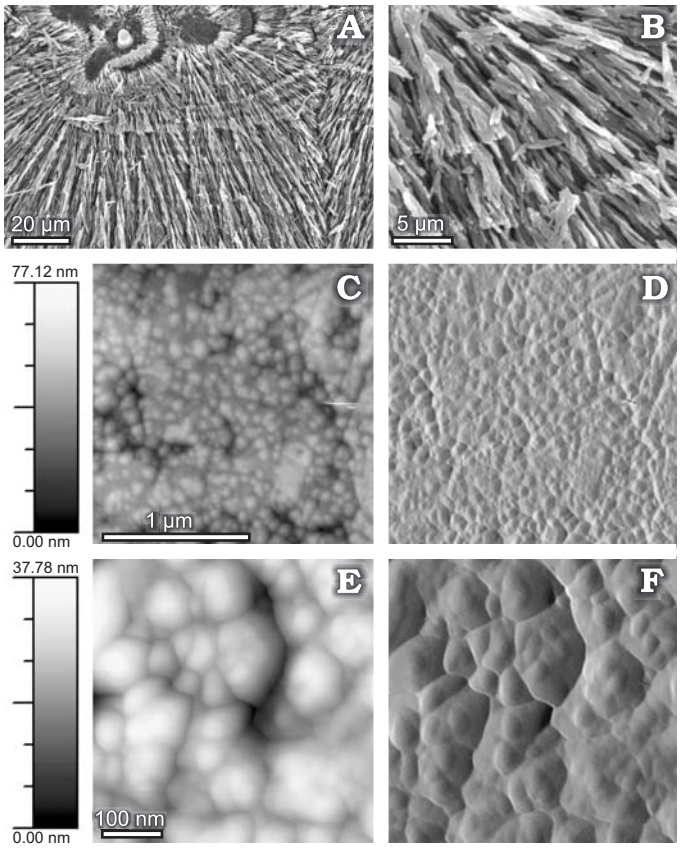

Fig. 2. Scleractinian *Favia stelligera* (Dana, 1846), Recent, Lizard Island (Great Barrier Reef, Pacific Ocean), depth 5–10 m; ZPAL V.31/1 (fragment of colony collected by Ann Budd). Polished and etched (formic acid, 1%, 20s) septum with aragonite fibers in two (**A**, **B**) enlargements; note negative relief of etched organic components in dRAF zone (upper A) and between fiber's layers. AFM (contact mode; buffered pH = 8, ammonium persulfate 1%, 10 min.): height-2D projection (**C**, **E**), and deflection (**D**, **F**) images of 2×2 µm (C, D) and 500×500 nm (E, F) skeletal surface. Nanograins ca. 50–100 nm in diameter. Grayscale bars (left) show z-scale (height) of 2D projection images.

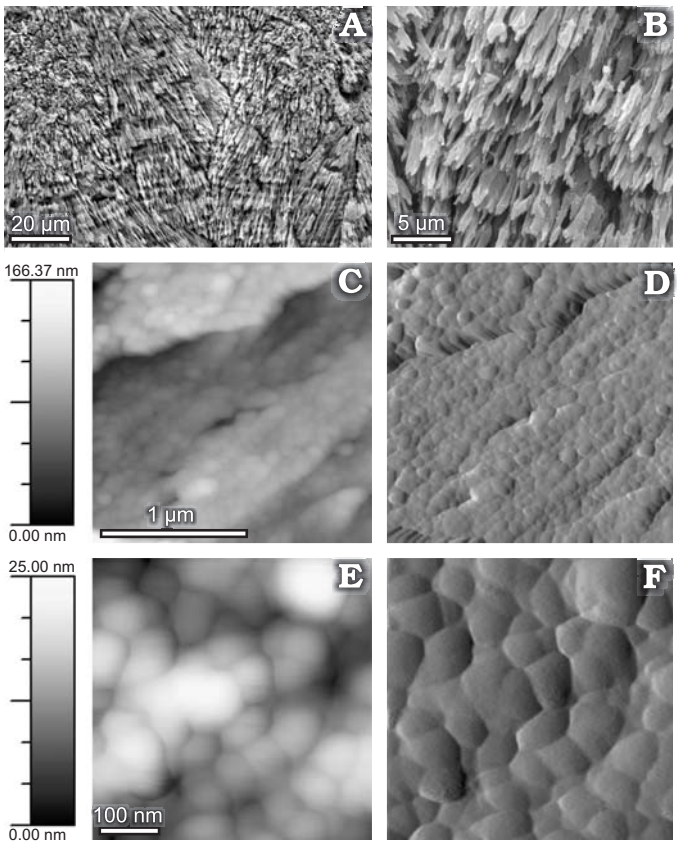

Fig. 3. Scleractinian *Goniastrea retiformis* (Lamarck, 1816), Recent, Saipan (Cloud Locality A-12, Northern Mariana Islands, Pacific Ocean); ZPAL V.31/2. Polished and etched (formic acid, 1%, 20s) septum with aragonite fibers in two (**A**, **B**) enlargements; note negative relief of etched organic components within fibers. AFM (contact mode; buffered pH = 8, ammonium persulfate 1%, 10 min.): height-2D projection (**C**, **E**), and deflection (**D**, **F**) images of 2×2 µm (C, D) and 500×500 nm (E, F) skeletal surface. Nanograins ca. 50–100 nm in diameter. Grayscale bars (left) show z-scale (height) of 2D projection images.

Synthetic calcium carbonate crystals

The AFM pictures of aragonite crystals prepared synthetically reveal the presence of terraces, usually a few hundred nanometers width. The surface of the terraces, before and after treatment with oxidizing solution (1% ammonium persulfate), did not exhibit nanograin texture (Fig. 1E–G); occasionally the surface of unprocessed or chemically processed crystals had a slightly rippled texture (particularly visible on deflection images Fig. 1F, H).

Extant calcium carbonate biocrystals

Microscale.—The main microcomponent of the aragonite skeleton of examined zooxanthellate scleractinians, i.e., *Favia stelligera* (Dana, 1846), Fig. 2A, B and *Goniastrea retiformis* (Lamarck, 1816), Fig. 3A, B, consist of fibers whose larger bundles radiate from calcification centers (CRA *sensu* Stolarski 2003 or Early Mineralization Zone *sensu* Cuif et al. 2003). In acidic etched samples, fibers are regularly tappered in radial direction (every ca. 3–5 µm).

The basal calcite skeleton of calcareous sponge (*Petrobiona massiliana* Vacelet and Lévi, 1958; Fig. 4A, B) and aragonite skeleton of a stylasterid (*Adelopora fragilis* Cairns, 1991; Fig. 5A, B) consist of fibers organized into spherulitic structures (*P. massiliana*) or coenosteal layers (*A. fragilis*). In magnifications comparable to those used for capturing of scleractinian skeleton, sponge and stylasterid fibers do not exhibit dense, regular tapered in etching relief (Figs. 4A, 5A). Although, the skeleton of *P. massiliana* was prepared using exactly the same etching protocol as the rest of the samples, the calcite fibers are not discretely separated from each other as are aragonite fibers in scleractinian samples. Also fibers of stylasterid coenosteum were less discretely separated in comparison to scleractinian fibers.

Nanoscale.—The aragonitic mineral phase of skeletal fibers of extant scleractinians consists entirely of nanograins ca. 50–100 nm in diameter separated from each other by spaces of a few nanometers width (Figs. 2C–F, 3C–F). Individual

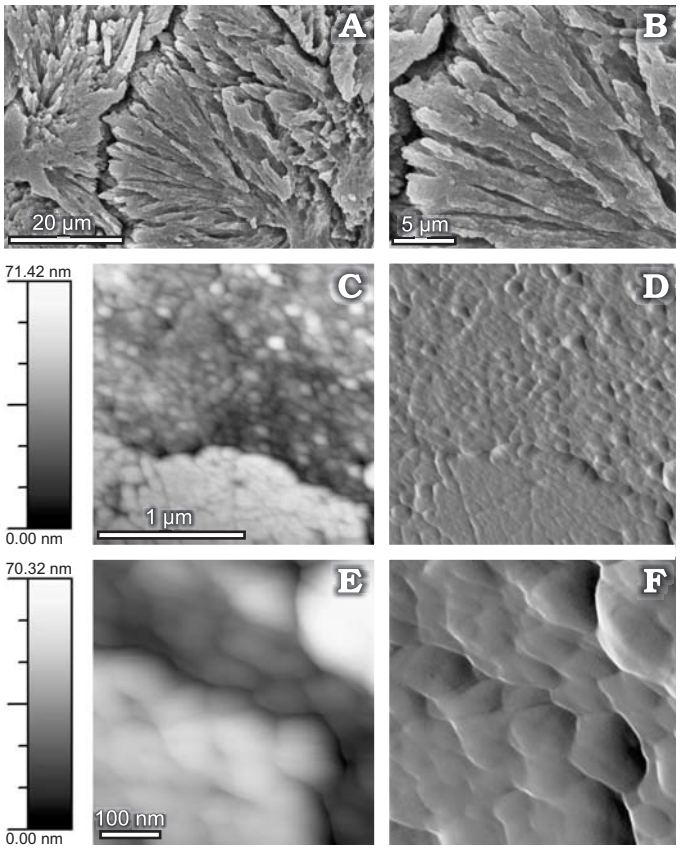

Fig. 4. Calcareous sponge *Petrobiona massiliana* Vacelet and Lévi, 1958, Recent, Marseille, submarine cave, "Grotte du Figuier", depth 10 m; ZPAL V.31/3. Polished and etched (formic acid, 1%, 20s) basal skeleton (spherulites) with calcite fibers; two enlargements (**A**, **B**). AFM (contact mode; buffered pH = 8, ammonium persulfate 1%, 10 min.): height-2D projection (**C**, **E**), and deflection (**D**, **F**) images of 2×2 µm (C, D) and 500×500 nm (E, F) skeletal surface. Nanograins ca. 50–100 nm in diameter. Grayscale bars (left) show z-scale (height) of 2D projection images.

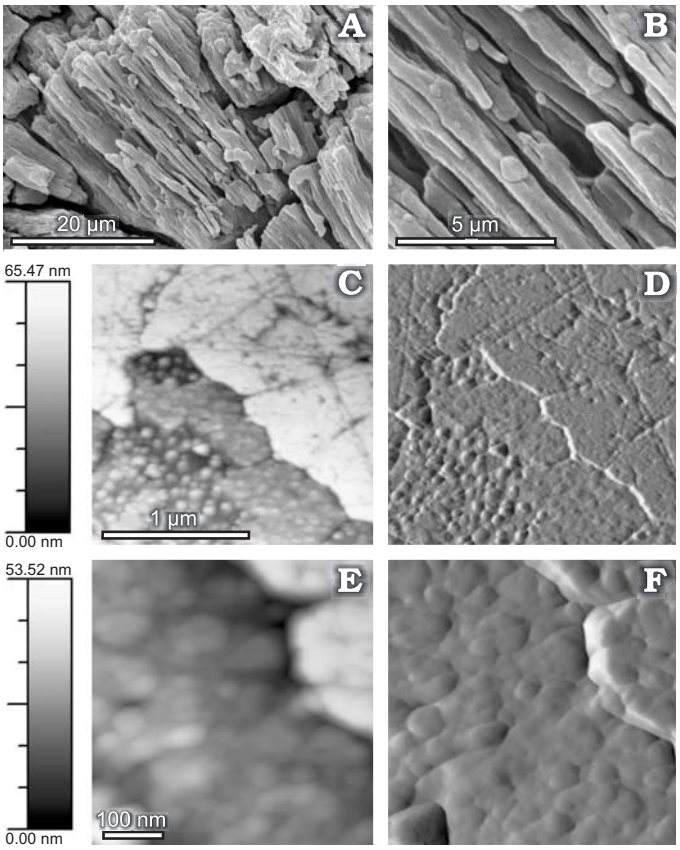

Fig. 5. Stylasterid *Adelopora fragilis* Cairns, 1991, Recent, New Caledonia, ORSTOM 5, DW 490, 18°54.9'S/163°24,3'E, depth 230 m; ZPAL V.31/4. Polished and etched (formic acid, 1%, 20s) coenosteum with aragonite fibers; two enlargements (**A**, **B**). AFM (contact mode; buffered pH = 8, ammonium persulfate 1%, 10 min.): height-2D projection (**C**, **E**), and deflection (**D**, **F**) images of 2×2 µm (C, D) and 500×500 nm (E, F) skeletal surface. Nanograins ca. 50–100 nm in diameter. Grayscale bars (left) show z-scale (height) of 2D projection images.

nanograins have a semicircular outline. Ocasionally, especially in the skeleton of *F. stelligera*, slightly larger, ca. 100–200 nm, rounded structures are observed but they appear to be the aggregates of common smaller nanograins, ca. 50–80 nm in diameter (Fig. 2E, F).

The nanograins revealed in calcite fibers of the basal skeleton of the calcareous sponge *P. massiliana* and aragonite coralla of the stylasterid *A. fragilis* (Figs. 4C–F and 5C–F, respectively) have the same size and are arranged identically as those in scleractinian samples. In places, the surface of AFM scanned material shows regions named herein "floes" (or having "floe-like texture") with weaker relief (z-scale) and nanograins not so clearly separated from each other though recognizable, especially at higher magnifications. The surface of the "floe" regions often displays scratches due to grinding.

Fossil aragonite biocrystals

Microscale.—In polished and etched sections, aragonite fibers are discretely separated from each other in coralla of the Miocene *Paracyathus cupula* Reuss, 1871 (Fig. 6A, B), Oxfordian *Isastraea* cf. *bernensis* Étallon in Thurmann and Étallon, 1864 (Fig. 9A, B) and a Carnian unidentified tropiastraeid; (Fig. 10A, B.) they do not differ morphologically from their recent counterparts. Fibers are more weakly separated in the skeleton of the Santonian *Rennensismilia complanata* (Goldfuss, 1826) and Cretaceous *Trochocyathus egericus* (White, 1879); Figs. 6A, C and 7A, B, respectively. In skeleton of the Carnian *Pachysolenia cylindrica* Cuif, 1975 fibers are poorly separated, and slender fibers are regularly interposed with broader crystals (Fig. 11A, B). In *I.* cf. *bernensis* (Fig. 9B) and *R. complanata* (Fig. 7B), in places, regular discontinuities were observed between layers of fibers, though the main part of the fibrous region of the corallum of *R. complanata* does not here exhibit the illustrated pattern. Also aragonite fibers in skeleton of *P. cupula* are tapered but irregularly as in extant members of this genus [Stolarski, unpublished data: *Paracyathus pulchellus* (Philippi, 1842); see also Cairns et al. 1999] and other extant azooxanthellate corals examined (Stolarski 2003). Fibers in *T. egericus* and *R. complanata* occasionally show very distinct (radially) but discontinuous gaps (laterally), which most likely represent cracks in the material.

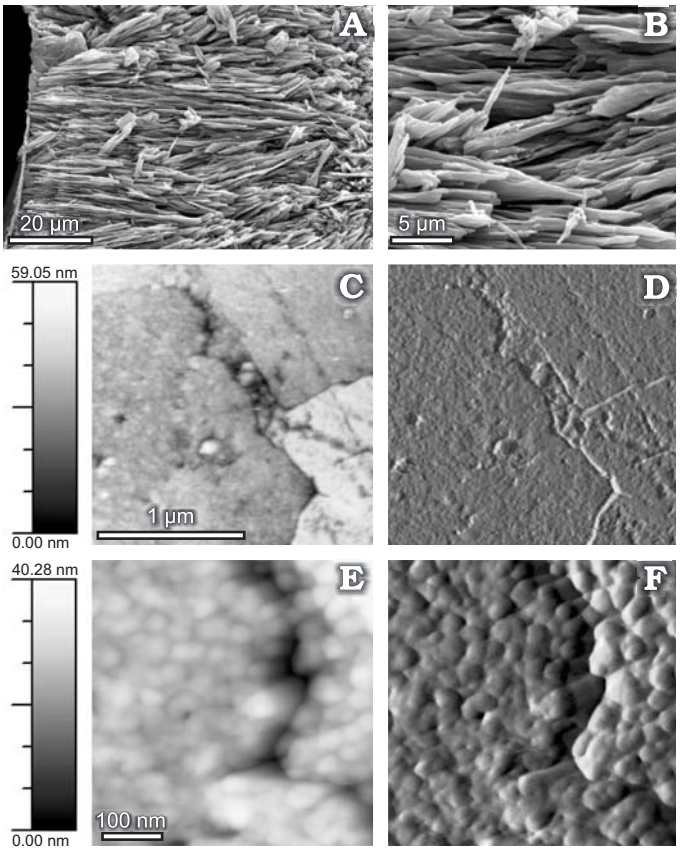

Fig. 6. Scleractinian *Paracyathus cupula* Reuss, 1871, Miocene (Neogene), Korytnica, Holy Cross Mts, Poland; ZPAL V.31/5. Polished and etched (formic acid, 1%, 20s) septum with aragonite fibers; two enlargements (**A**, **B**). AFM (contact mode; buffered pH = 8, ammonium persulfate 1%, 10 min.): height-2D projection (**C**, **E**), and deflection (**D**, **F**) images of 2×2 µm (C, D) and 500×500 nm (E, F) skeletal surface. Nanograins ca. 50–100 nm in diameter. Grayscale bars (left) show z-scale (height) of 2D projection images.

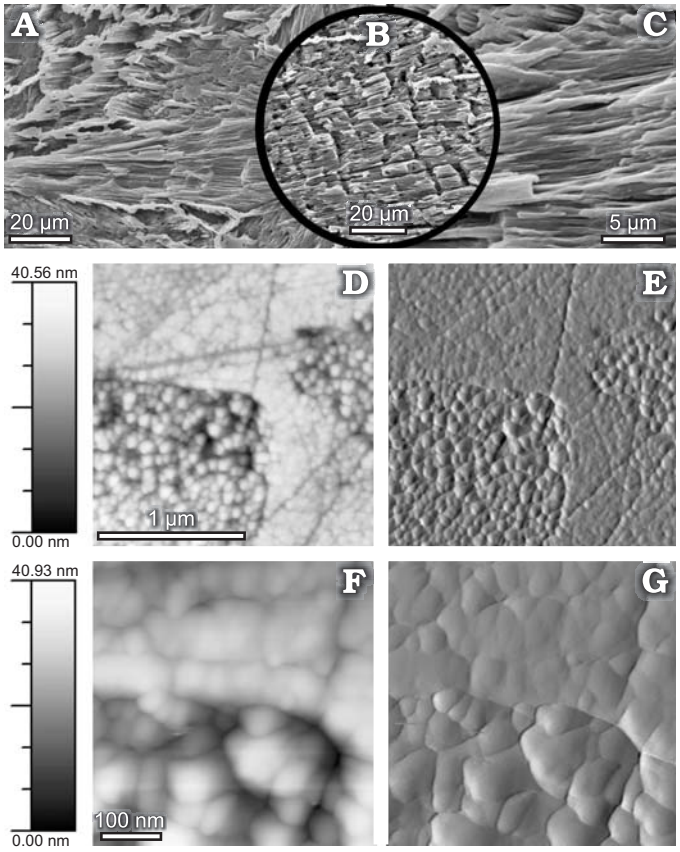

Fig. 7. Scleractinian *Rennensismilia complanata* (Goldfuss, 1826), Santonian (Upper Cretaceous), Lower Gosau beds, near Gosau, Austria; USNM 499247. Polished and etched (formic acid, 1%, 20s) septum with bundles of aragonite fibers enveloped by structures with positive etching relief interpreted by Sorauf (1999) as sheaths of proteinaceous matrix (**A**, **C**, same skeletal regions in different magnifications); in places skeletal etched fibers show regular discontinuities similar to that of extant zooxanthellates (**B**). AFM (contact mode; buffered pH = 8, ammonium persulfate 1%, 10 min.): height-2D projection (**D**, **F**), and deflection (**E**, **G**) images of 2×2 µm (D, E) and 500×500 nm (F, G) skeletal surface. Nanograins ca. 50–100 nm in diameter. Grayscale bars (left) show z-scale (height) of 2D projection images.

Nanoscale.—Particularly regularly distributed nanograins, ca. 50–100 nm in diameter separated from each other by spaces of a few nanometers, were observed in fibrous skeleton of the Oxfordian *I.* cf. *bernensis* and the Carnian tropiastraeid. (Figs. 9C–F and 10C–F, respectively). Aragonitic fibers of the Neogene (Miocene) coral *P. cupula* and Cretaceous corals *R. complanata* and *T. egericus* are nanogranular, although boundaries between individual grains are occasionally not well resolved (Figs. 6C–F, 7D–G, 8C–F, respectively). Conversely, the texture of the fibrous wall skeleton of *P. cylindrica* is bumpy but typical nanograins are not recognized in the several sites examined.

The skeletal surface of many fossil samples (except of *I.* cf. *bernensis* and the tropiastraeid) has, in places, a floe-like texture (i.e., areas with weaker relief and with less distinct borders between individual nanograins); borders between adjacent floes are often sharp. Occasionally, regions of floe-like structure adjoin skeletal zones with excellent development of nanogranular texture (Figs. 7D–G, 10C, D). Nanograins have not been recognized within skeletal "floes" of *P. cylindrica*.

Abiogenic calcium carbonate crystals

The calcite mineralogy of examined sparry calcite cements was determined by Feigl's solution and, in the examples illustrated, by XRD analysis.

Crystals of sparry calcite from interseptal spaces of upper Carnian corals from Alpe di Specie, Italy, and comparative calcite materials (sparry calcite from the Upper Jurassic fossils of Slovakia, and calcite karstic deposits of Poland) etched with oxidizing solution, showed rather smooth surfaces, occasionally with grinding scratches at the same AFM magnification range as used for biogenic samples. No nanograin texture was observed in these samples and z-scale values were very low (e.g., Fig. 12B).

Unexpectedly, we found nanograins ca. 60–100 nm in diameter (Fig. $12A_4$–A_7) in crystals of sparry calcite occurring in the interseptal spaces of a Maastrichtian scleractinian coral with entirely calcitic skeleton (XRD confirmed; detailed

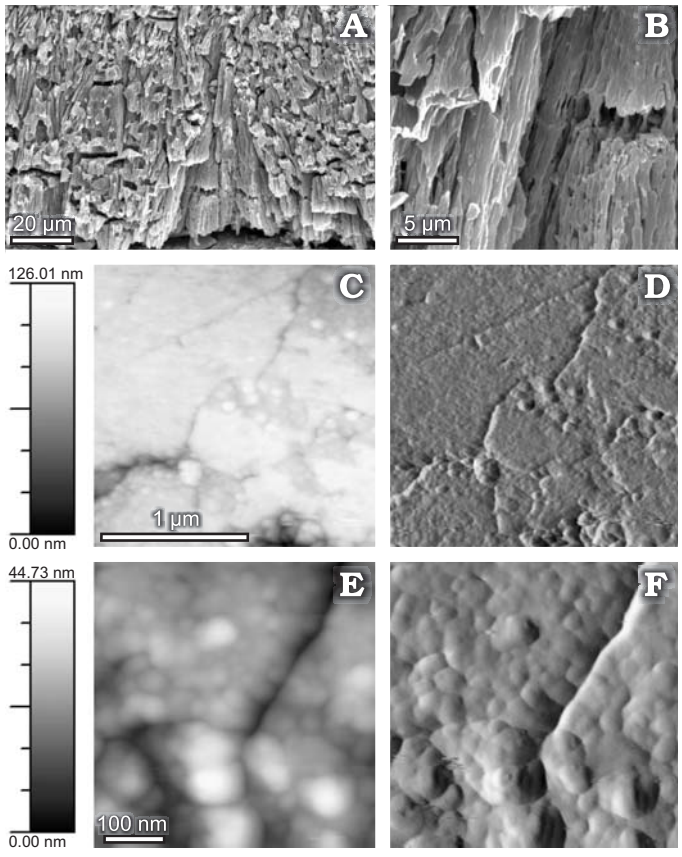

Fig. 8. Scleractinian *Trochocyathus egeri* (White 1879), Upper Campanian to Maastrichtian (Upper Cretaceous), Pierre shale (upper part), Dry Creek, Black Hills (South Dakota, USA); USNM 75221. Polished and etched (formic acid, 1%, 20s) septum with aragonite fibers; two enlargements (**A**, **B**). AFM (contact mode; buffered pH = 8, ammonium persulfate 1%, 10 min.): height-2D projection (**C**, **E**), and deflection (**D**, **F**) images of 2×2 µm (C, D) and 500×500 nm (E, F) skeletal surface. Nanograins ca. 40–100 nm in diameter. Grayscale bars (left) show z-scale (height) of 2D projection images.

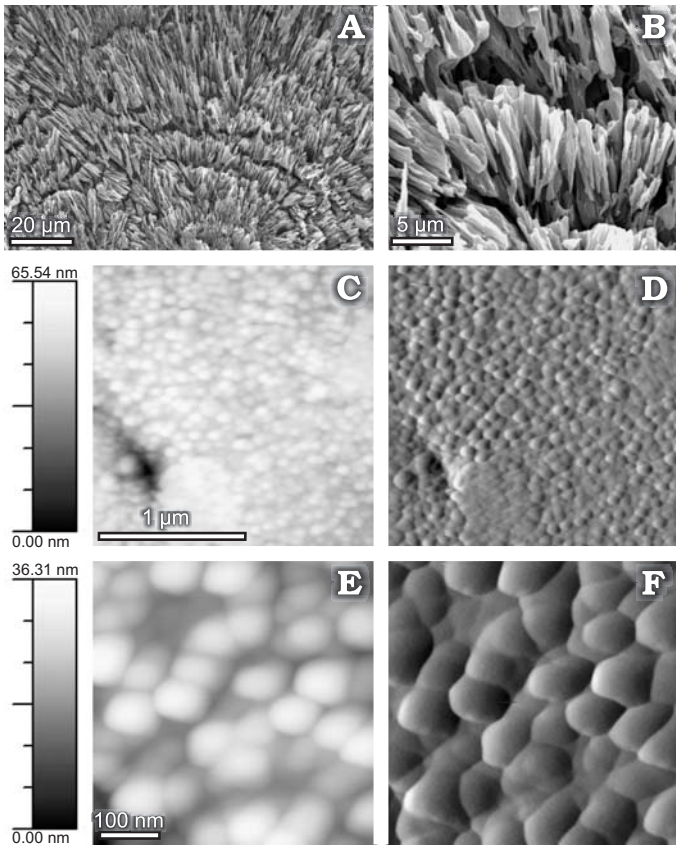

Fig. 9. Scleractinian *Isastraea* cf. *bernensis* Étallon in Thurmann and Étallon, 1864. Oxfordian (Upper Jurassic), Ostromice, western Pomerania, Poland; ZPAL H.IV/303. Polished and etched (formic acid, 1%, 20s) septum with aragonite fibers; two enlargements (**A**, **B**). AFM (contact mode; buffered pH = 8, ammonium persulfate 1%, 10 min.): height-2D projection (**C**, **E**), and deflection (**D**, **F**) images of 2×2 µm (C, D) and 500×500 nm (E, F) skeletal surface. Nanograins ca. 60 (commonly 80) –100 nm in diameter. Grayscale bars (left) show z-scale (height) of 2D projection images.

diagenetic history of this specimen will be published elsewhere). The individual nanograins are easily discernible (Fig. 12A$_6$, A$_7$) although boundaries between them are less distinct than in modern and some fossil biocrystals (e.g., Figs. 2E, 3E, 6E, 7D, 9C, 10C). AFM observations were repeated in different regions of the sparry calcite infilling showing the same nanogranular pattern of the crystal surface. The surface of the sample was generally smooth (low values of the z-scale Fig. 12A$_4$–A$_7$, but higher than of sparry calcite crystals without discernible nanograins), but with prominent grinding scratches (Fig. 12A$_4$, A$_5$). Back-scattered electron microscopy images of some of the examined crystals indicate a complex crystallization history (Fig. 12A$_2$, with at least two phases of growth) but details of this are out of the scope of this report.

Biogeochemistry of the biocrystals: a preliminary survey

We conducted a preliminary survey of some microscopically, geochemically and thermogravimetrically detectable parameters of selected samples that may provide some insight into their overall preservation status. The selection comprised of four specimens with easily discernible nanogranular structure of fibers (Recent *F. stelligera*, Cretaceous *R. complanata*, Jurassic *I.* cf. *bernensis*, and the Triassic tropiastraeid) along with a Triassic *P. cylindrica* that had a partly calcitized skeleton without distinct nanogranular structure. Skeletal fragments examined with MFM and WDS techniques are comprised of fibers (whose nanostructure were examined) and calcification centers (whose transformation is a sensitive marker of the early diagenetic changes of the skeleton; see Cuif and Dauphin 1998; Stolarski 2003). Three samples were also examined with thermogravimetric methods to assess any possible relationship between the presence of nanograins and the amount of thermally decomposed intraskeletal organic matter; samples analysed thermogravimetrically included: Recent *F. stelligera* (extant skeleton with nanograins), Jurassic *I.* cf. *bernensis* (fossil skeleton with nanograins), and the Triassic *P. cylindrica* (fossil skeleton without nanograins).

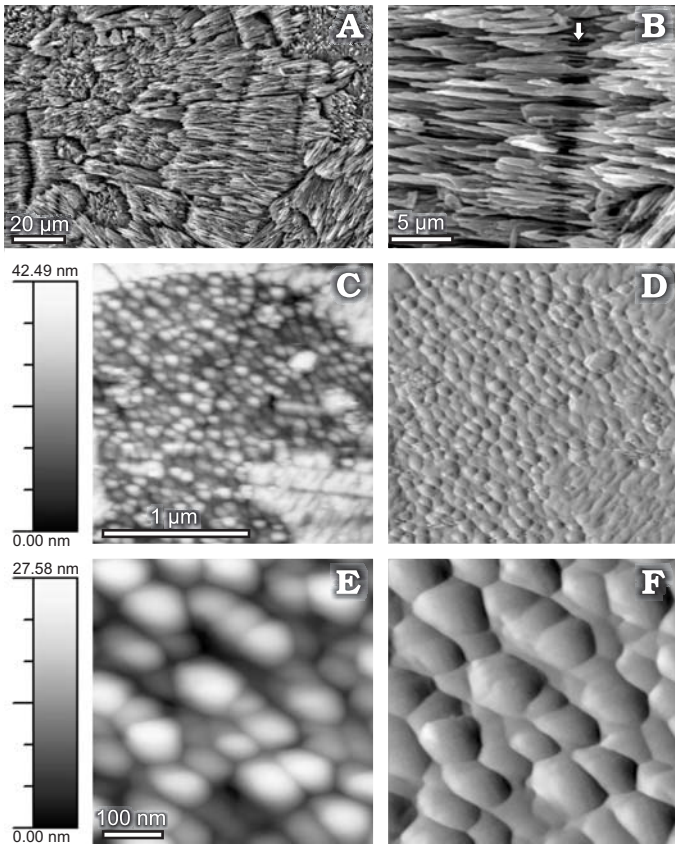

Fig. 10. Tropiastraeid scleractinian, undetermined. Upper Carnian (Upper Triassic), Alpe di Specie, Dolomites, Italy; ZPAL V.31/6. Polished and etched (formic acid, 1%, 20s) septum with aragonite fibers; two enlargements (**A**, **B**); fiber's tapering (e.g., arrow in B) is possibly related to original organic matter enrichment zones. AFM (contact mode; buffered pH = 8, ammonium persulfate 1%, 10 min.): height-2D projection (**C**, **E**), and deflection (**D**, **F**) images of 2×2 µm (C, D) and 500×500 nm (E, F) skeletal surface. Nanograins ca. 60 (commonly 80) –100 nm in diameter. Grayscale bars (left) show z-scale (height) of 2D projection images.

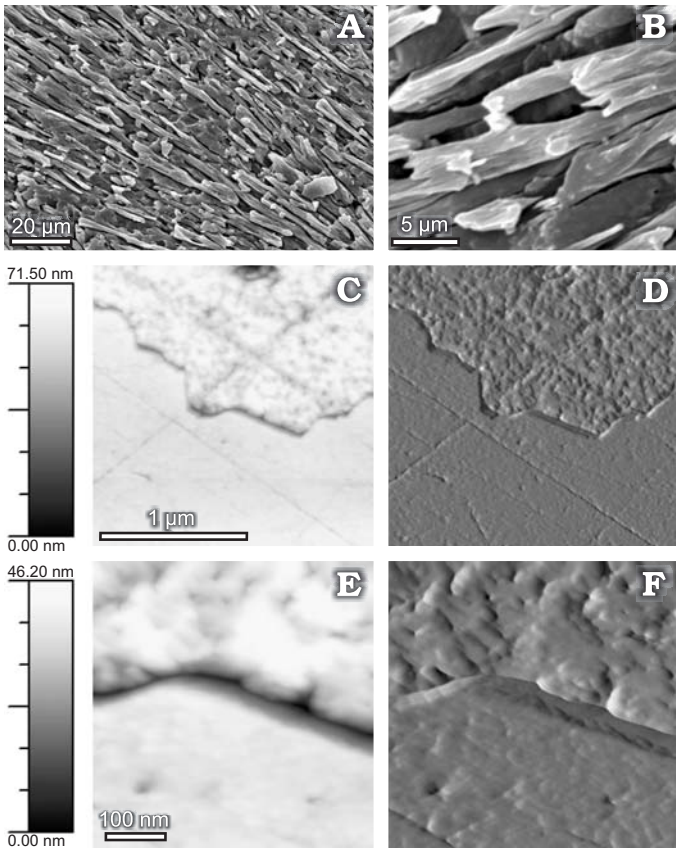

Fig. 11. Scleractinian *Pachysolenia cylindrica* Cuif, 1975, lower Norian (Upper Triassic), Alakir Çay, Turkey; ZPAL V.31/7. Polished and etched (formic acid, 1%, 20s) pachythecal wall consisted of aragonite fibers; two enlargements (**A**, **B**). AFM (contact mode; buffered pH = 8, ammonium persulfate 1%, 10 min.): height-2D projection (**C**, **E**), and deflection (**D**, **F**) images of 2×2 µm (C, D) and 500×500 nm (E, F) skeletal surface. Skeletal regions that show effects of oxidizing solution action (upper part of images) do not exhibit distinct nanogranular pattern. Grayscale bars (left) show z-scale (height) of 2D projection images.

Light microscope and MFM.—Different optical properties of the thickening fibers and "centers of calcification" are clearly visible in the three samples: (1) Recent *F.steligera*: browhish, "beads" of calcification centers generally separated from each other in the mid-septal region of transversely sectioned septa *versus* usually transparent, colorless bundles of fibers with dense and regular darker alternations (Fig. $13A_1$); (2) Cretaceous *R. complanata*: grey-brown, homogenous mid-septal zone and more or less transparent bundles of fibers radiating from the mid-septal region, but not showing distinct darker alternations (Fig. $13B_1$); (3) Triassic *P. cylindrica*: very distict, transparent mid-septal zone, and fibrous zones of septa and wall, transparent but not homogenously colored and lacking distinct darker alternations (Fig. $13E_1$). In two samples calcification centers are not well differentiated but bundles of fibers are organized around these regions: these are the Upper Jurassic *I.* cf. *bernensis* (4) and the Triassic tropidastraeid (5); Figs. $13C_1$, D_1, respectively.

In MFM, only the mid-septal region with calcification centers of Recent *Favia stelligera* showed a prominent yellowish-green chromatic response, whereas the adjacent zone of thickening fibers exhibited only delicate greenish-orange "glow" (Fig. $13A_2$); the fluorescent response of all fossil skeletons was very weak and not characteristic, and regions with calcification centers did not differentiate from other regions.

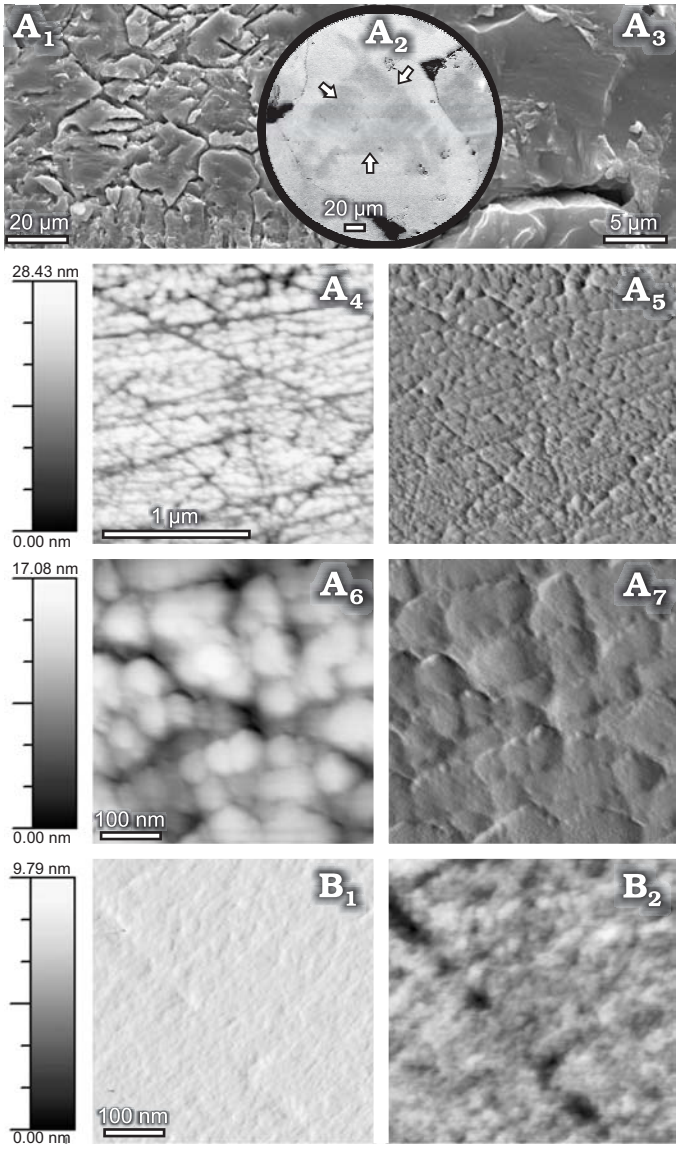

Fig. 12. Sparry calcite developed between septa of fossil scleractinian corals. **A**. ZPAL V.31/8 (lower Maastrichtian, Upper Cretaceous, Lubycza Królewska, Lublin Upland, eastern Poland). **B**. ZPAL V.31/9 (Carnian, Upper Triassic, Alpe di Specie, Dolomites, Italy). Polished and etched (formic acid, 1%, 20s) ZPAL V.31/8 sparry calcite in two enlargements (A_1, A_3). Back-Scattered Electron Microscopy image (A_2) shows complex history of idividual calcite grain, highlighting zones of different elemental composition: those with elements of lower atomic numbers are darker (core of the grain outlines with arrows), whereas those of higher atomic numbers are lighter (outer part). A_4–A_7, B_1, B_2, AFM (contact mode; buffered pH = 8, ammonium persulfate 1%, 10 min.): height-2D projection (A_4, A_6, B_1), and deflection (A_5, A_7, B_2) images of 2×2 µm (A_4, A_5) and 500×500 nm (A_6, A_7, B_1, B_2) sample surface. Nanograins on A_4–A_7 are ca. 60–100 nm in diameter. Grayscale bars (left) show z-scale (height) of 2D projection images.

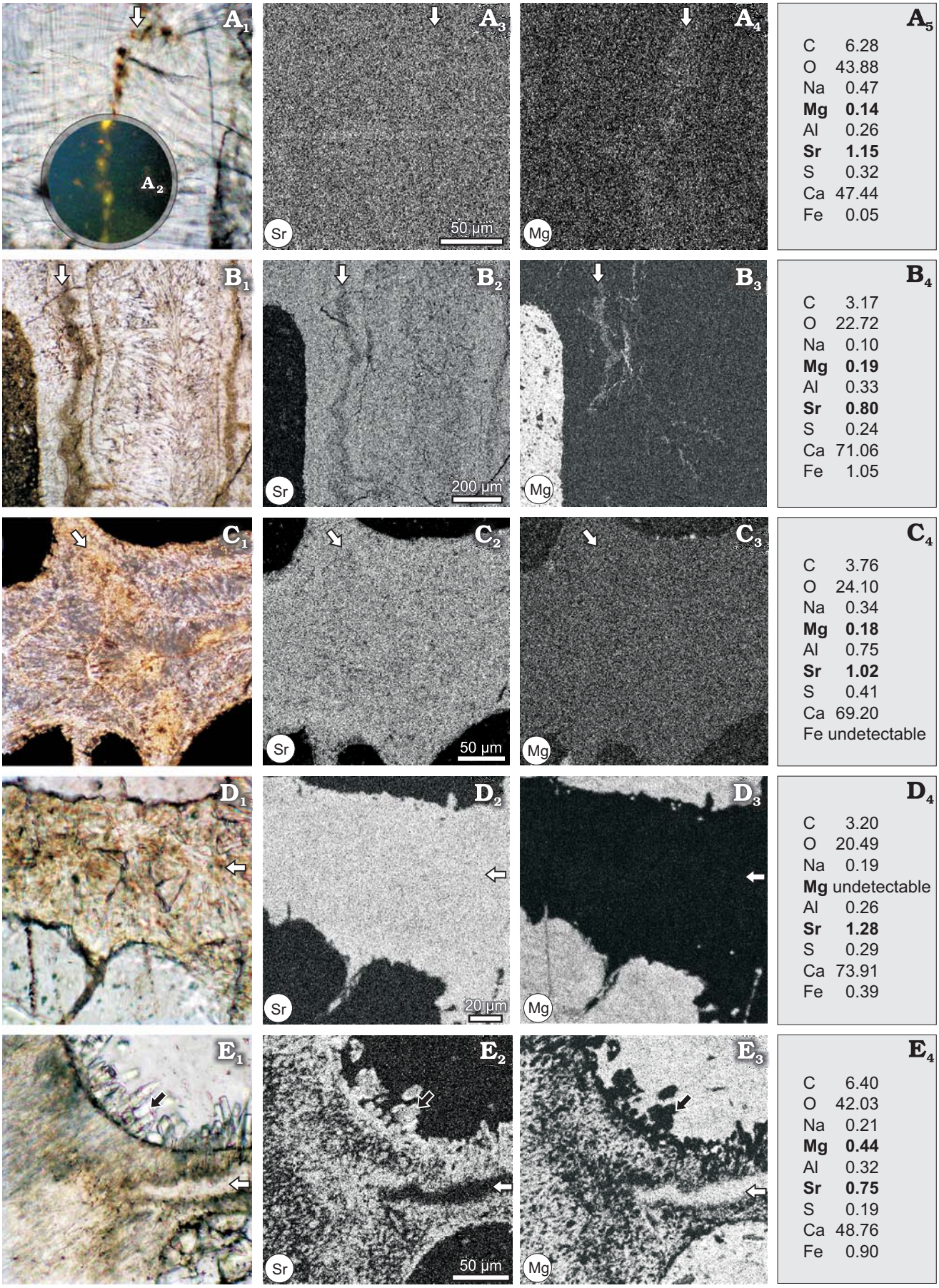
A1
A2
A3
Sr
50 µm
A4
Mg
A5
C 6.28
O 43.88
Na 0.47
Mg 0.14
Al 0.26
Sr 1.15
S 0.32
Ca 47.44
Fe 0.05
B1
B2
Sr
200 µm
B3
Mg
B4
C 3.17
O 22.72
Na 0.10
Mg 0.19
Al 0.33
Sr 0.80
S 0.24
Ca 71.06
Fe 1.05
C1
C2
Sr
50 µm
C3
Mg
C4
C 3.76
O 24.10
Na 0.34
Mg 0.18
Al 0.75
Sr 1.02
S 0.41
Ca 69.20
Fe undetectable
D1
D2
Sr
20 µm
D3
Mg
D4
C 3.20
O 20.49
Na 0.19
Mg undetectable
Al 0.26
Sr 1.28
S 0.29
Ca 73.91
Fe 0.39
E1
E2
Sr
50 µm
E3
Mg
E4
C 6.40
O 42.03
Na 0.21
Mg 0.44
Al 0.32
Sr 0.75
S 0.19
Ca 48.76
Fe 0.90

WDS mapping.—In *F. stelligera*, there are no sharp differences in Mg and Sr distribution patterns, however, light strip-like concentrations of Mg, parallel to the septum edge can be recognized (Fig. 13A_4); higher concentration of Mg (and zone slightly depleted in respect to Sr) is visible along the mid-septal zone (white arrow in Fig. 13A_3, A_4).

In Cretaceous *R. complanata* mid-septal region is clearly enriched in respect to Mg and, respectively, depleted in respect of Sr (Fig. 13B_2, B_3); almost the entire region where calcareous sediment fills in the interseptal space (on the left) bears strong Mg signal.

In the Jurassic *I.* cf. *bernensis* and the Triassic tropidastraeid, distribution of Mg and Sr is even more homogenous than in *F. stelligera* without any clear-cut pattern (Fig. 13C_2, C_3, D_2, D_3), but in the tropidastraeid the Mg signal, in comparison to Sr, is very low. Sparry calcite crystals that fill in the interseptal space in tropidastraeid corallum bear a very distinct Mg signal.

In the Triassic *P. cylindrica*, distribution of Sr and Mg shows a spotted pattern. Regions depleted in Sr are respectively enriched in Mg, especially distinct in the mid-septa zone; Fig. 13E_2, E_3. Crystals of fibrous cement developed on the septal surface (Fig. 13E_1–E_3, black arrow) are enriched in Sr and depleted in Mg. Sparry calcite crystals of interseptal infilling bear a very distinct Mg signal.

Bulk EDS analysis (Fig. 13A_5, B_4, C_4, D_4, E_4).—The bulk EDS analysis of the fibrous regions shows that the weight percents of Sr ranges from 0.75 (*R. complanata*) to 1.28 (Triassic tropidastraeid); in extant *F. stelligera* the weight percent value of Sr is 1.15. The Mg weight percent ranges from an undetectable amount in the tropidastraeid to 0.44% in *P. cylindrica*; by comparison, the weight percent of this element in *F. stelligera* is 0.14.

Thermogravimetry.—Weight loss related to thermal decomposition was calculated based on a direct thermogravimetrical curve (TD). The weight loss curve for the synthetic aragonite that was used for comparisons is generally flat until rapid weight loss attributed to $CaCO_3$ decomposition to CaO above 600°C (Fig. 14A). The weight loss curve for *P. cylindrica* is rather flat at the beginning of the measurement (Fig. 14B) but showing a shallow though distinct drop at ca. 340°C; the drop is correlated with shallow endotherm peak in differential thermogravimetrical (DTA) curve. Calculated weight loss at this region is ca. 3 milligrams. The weight loss curve for *I.* cf. *bernensis* (Fig. 14C) shows a distinct drop at ca. 370°C correlated with endotherm peak followed by small exotherm elevation in DTA curve (at ca. 420°C). Calculated weight loss at this region is ca. 7 milligrams. The weight loss curve for *F. stelligera* is a little steeper from the beginning of the measurement in comparison to other samples (Fig. 14D) and shows distinct drop at ca. 300°C which correlates with endotherm peak in DTA curve. This event is followed by exotherm elevation at ca. 360°C. Calculated weight loss at this region is ca. 6 milligrams. Rapid weight loss attributed to $CaCO_3$ decomposition to CaO and CO_2 emission starts >700°C in all four samples.

Discussion

Formation of the skeleton involves mutual synergistic interactions between organism-related ("vital effect") and external environmental factors. These factors operate differently at various levels of skeletal structural hierarchy: some that strongly influence biomineral formation at the macroscale can be ignored at a micro-scale and *vice versa*. For example, although it is possible to simplify anatomical and environmental constraints influencing the overall shape of a bone (muscle attachments, weight of the body, etc), the causal links between organismal and environmental factors that control micro- and nanoscale phenomena of bone formation require explanation of the developmental, biochemical and physical mechanisms that control the arrangement of osteocytes, formation of collagen fibrils, shape of hydroxyapatite crystals, etc. In the two following chapters we discuss a broader context of organism-related *versus* external-environmental factors that may influence the micro- and nanoscale structures illustrated in this paper.

Microscale skeletal fibers

Many organism-related factors have a direct influence on skeletal microstructural patters, and it is intuitively expected that more refined means for this control occur in organisms of more complex rather than simpler body organization plans, physiologies, etc. Indeed, in invertebrates that produce microstructurally complex skeletons (e.g., mollusks with composite shell layers of different mineralogy) biochemically diverse protein molecules also have been identified that strongly affect biocrystal formation (see overview by Marin and Luquet 2004).

Conversely, much simpler microstructural patterns in skeletons of "primitive" calcareous algae, sponges and cnidarians may suggest a dominance of physico-chemical over biological factors in controlling mineralization and, indeed, such a model was proposed for the formation and spatial arrangement of aragonitic fibers in scleractinian coralla (Bryan

← Fig. 13. Overall geochemical characteristics of some scleractinian samples used in this report: **A**. Recent *Favia stelligera*, ZPAL V.31/1. **B**. *Rennensismilia complanata*, USNM 499247. **C**. *Isastraea* cf. *bernensis*, ZPAL H.IV/303. **D**. Tropiastraeid, unidentified, ZPAL V.31/6. **E**. *Pachysolenia cylindrica*, ZPAL V.31/7. Transverse section of septum in TLM views (A_1, B_1, C_1, D_1, E_1); greyscale Sr (A_3, B_2, C_2, D_2, E_2) and Mg (A_4, B_3, C_3, D_3, E_3) WDS mappings—darker areas equal low concentration whereas lighter areas equals higher concentration of element; bulk EDAX elemental quantitative analysis of fibrous septal regions (A_5, B_4, C_4, D_4, E_4: bold values mark elements used as preservation proxies). Organic matter concentrated along RAF zone of Recent *F. stelligera* exhibits light, green-yellow fluorescence (A_2: MFM view) whereas no distinct response is reported from fossil samples. RAF (CRA) regions in all septa marked with white arrows. Acicular aragonite cement formed on septal surface of *P. cylindrica* (E) marked with black arrow.

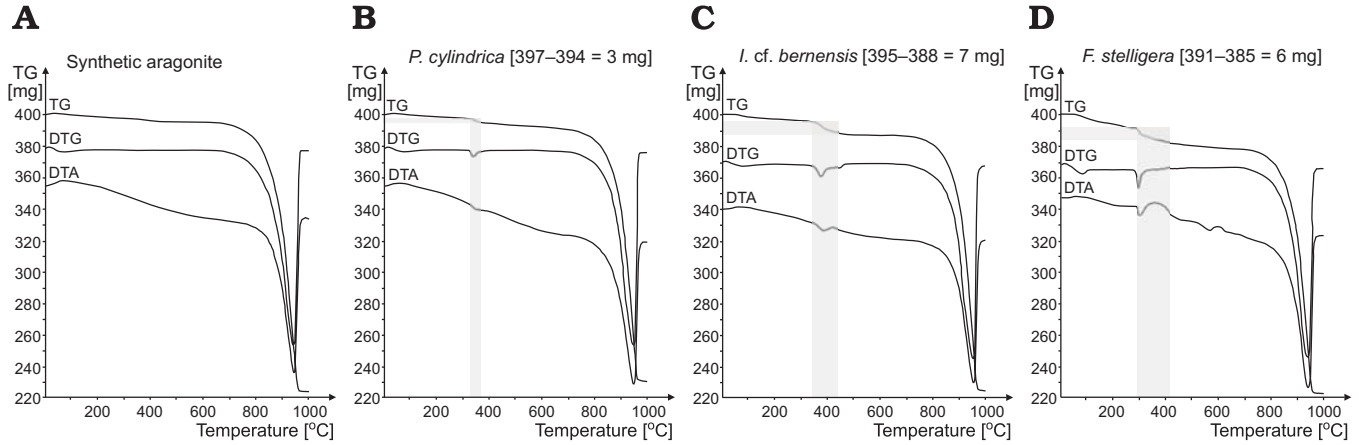

Fig. 14. Thermograms showing direct thermogravimetrical (TG; milligrams), differential thermogravimetrical (DTG; arbitrary units), and differential thermo-analytical (DTA; arbitrary units) curves of synthethic aragonite (**A**) and three samples with two different nanostructural patterns: Triassic *Pachysolenia cylindrica* (**B**) without distinct nanograins; Jurassic *Isastraea* cf. *bernensis* (**C**) and Recent *Favia stelligera* (**C**) with well developed nanograins. Assumed amount of intraskeletal hydrated organic components was calculated based on distinct weight loss of 400 mg sample that occurred at ca. 300–450°C.

and Hill 1941). Their model assumed an analogy with purely inorganic crystallization, and interpreted the skeletal fiber as a "single orthorhombic crystal of Aragonite" that "arise in a colloidal matrix secreted by, but external to, the ectoderm." According to their model, growth of fibers follows inorganic spherulitic crystallization: crystallization starts at nucleation points called "centers of calcification" and resulting bundles of fibers fill in available space (see also Barnes 1970: 1305). The organic components that were present (as assumed by Bryan and Hill, 1941: 86) in the skeleton originated from the decomposition of parent gel (colloidal matrix).

This model existed without any competing models for many years, occasionally being emended by a new data. For example, Wainwright (1964) demonstrated that fibers considered individual crystal units, actual are polycrystalline aggregates with ordered c-axis and randomly distributed a and b axes. Still in 1986, Constantz (1986a: 155) stated that the growth of skeletal aragonitic fibers and their organization into bundles "are entirely predictable by factors controlling abiotic, physiochemical crystal growth", however, noted also that the different diameter of aragonitic fibers (0.05–0.7 micrometers) and distribution of calcification centers can be taxon-related (thus clearly accepting the possibility of some biologically-related factors controlling mineralization[2]).

The coexistence of organic and mineral phases was long acknowledged (e.g., Bryan and Hill 1941: 86) but only more recently, work by Johnson (1980), but especially Cuif and co-authors (see overview Cuif and Sorauf 2001) has emphasized that microstructural organization of the mineral phase is strictly controlled by a spatial arrangement of the organic compounds that are incorporated later into the skeletal structure. These matrices show remarkable taxon- and physiologically-related variability (Cuif et al. 1997; Cuif et al. 1999), and calcium binding properties (Watanabe et al. 2003). This "biological spirit" in the interpretation of skeletal structures in Scleractinia manifests itself in a radical shift of emphasis in the model of biomineralization for "primitive" organisms. It is the organic framework produced by the organism that dictates arrangement of the mineral phase and not *vice versa*. This new perspective suggests a causal link between organismal genetics that regulates also biochemical properties of organic matrices and minute scale organization of the skeleton. Such a link is encouraging for paleontologists seeking congruence between molecular and morphological phylogenetic hypotheses by using new microstructural taxonomic criteria (e.g., Cuif et al. 1997: fig. 4; Stolarski 2003: 525; Cuif et al. 2003).

Skeletal fibers are, according to a new model, considered "matrix-mediated biominerals built by repeatedly produced micron-thick growth layers" (Cuif and Dauphin 2005a: 69). A consequence of this is that a single fiber consists of multiple superimposed smaller units that independently record physiological and environmental signatures ("environment recording units" as proposed by Cuif and Dauphin 2005a). For zooxanthellate corals, the smaller unit (a few to a dozen micrometers long) has a time equivalent of a day, whereas this time is probably longer for azooxanthellate corals (Stolarski 2003). As a result, traditional (EDS, WDS, micromilling, or laser ablation techniques for atomic spectroscopy) analytical methods with spatial resolution lower than 1 micrometer, allow one to obtain only averaged physiological/environmental proxies, sufficient for a global geochemical considerations but not useful for more subtle skeletal ap-

[2] According to Cohen and McConnaughey (2003), differences in fiber's morphology that Constantz (1986b) observed reflect rather different crystal growth rates than direct biological control over their geometry. For example, crystals of various minerals formed abiotically, are slender during fast crystallization whereas during longer growth they form thicker fibers. Actually, Constantz (1986b) observed slender crystals in fast growing acroporids, whereas thicker fibers occurred in exhibiting slower growing faviids.

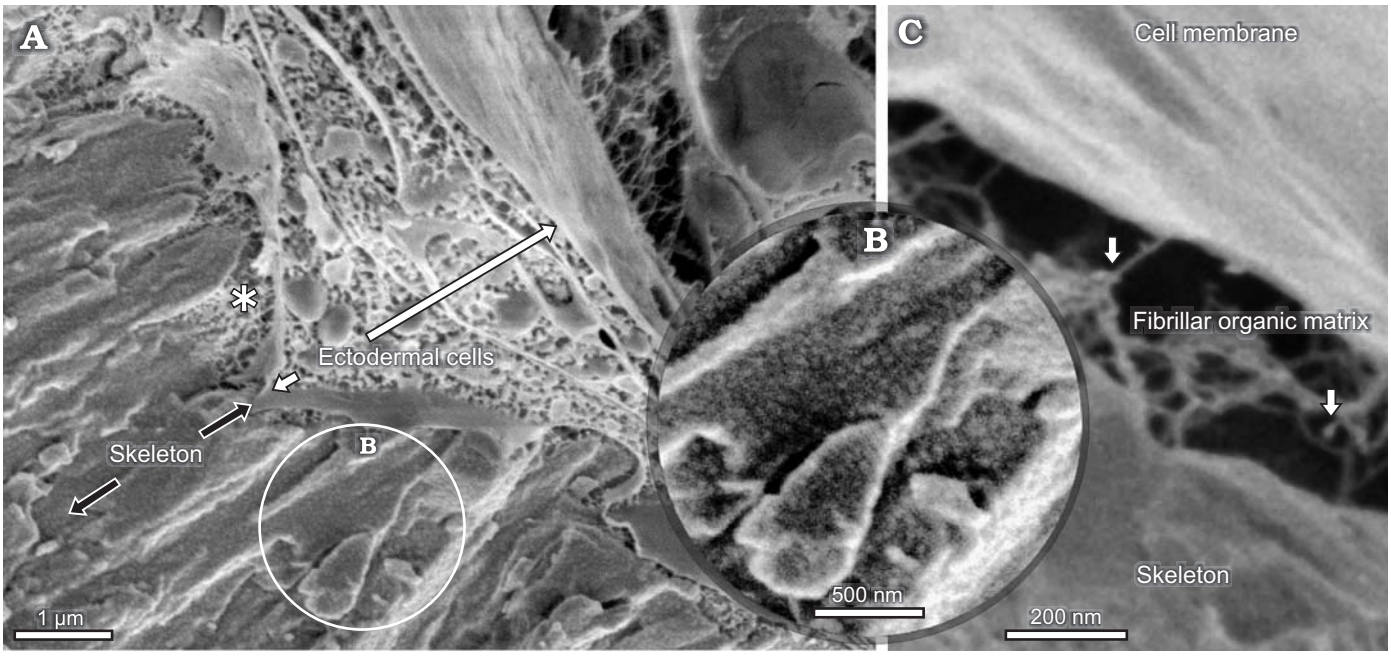

Fig. 15. *Galaxea fascicularis* (Linnaeus, 1767), skeleton and calicoblastic layer interface. **A**. FESEM image (reproduced after Clode and Marshall 2003a: figs. 1, 2) of frozen-hydrated specimen showing: nanogranular structure (**B**, close-up) of calcareous fibers at their entire length (non-etched state), cross-sections of spindle ectodermal cells with spherical intercellular vesicles, and fibrillar organic matrix (asterisk). **C**. Close-up of mesh-like, fibrillar organic matrix at skeleton-ectoderm interface with attached small nodular structures (white arrows) that, most likely, correspond to calcium enriched regions indicated by X-ray analysis.

proaches (e.g., diurnal change). Only the new analytical instruments permitting 50 nm spatial resolution (e.g., NanoSims) are capable of mapping the variability of diurnal biogeochemical signatures (Meibom et al. 2004). Clearly, research on the interplay between physiological and environmental processes now can be conducted at the nanoscale level where interpretations are much more challenging than the microstructural one and require viewing from a broad, multidirectional research perspective. Below, we discuss evidence and interpretations of nanostructures in various calcareous materials that were the subject of this study and others that are available in the literature.

Nature of nanograins

Before the introduction of ultrahigh resolution microscopic techniques (AFM or FESEM), the minute-scale (occasionally called nanoscale) components were thought to be only the "seed crystals" of calcareous fibers in invertebrate skeletons. For example, Reitner (1992) noted that "seed crystals" of aragonite crystals of spherulites in the aragonitic basal skeleton of the coralline demosponge *Astrosclera* were components 30–50 nm in size. In Scleractinia, minute-scale components were recognized within "calcification centers" but the suggested size range of the mineral particles differed significantly between authors: from 10–100 Å (1–10 nm) in "seed nuclei" of Constantz (1986a: 154) to about 1 micrometer in diameter (Wainwright 1964: 219; Cuif and Dauphin 1998: 264). Based on our current knowledge, the most accurate description of minute-scale skeletal structures provided by Isa (1986: 92) showed on SEM images that spherule crystals in subepithelial space are "about 1 µm in diameter and consisted of many finely granulated substructures of about 50 nm".

The introduction of FESEM allowed Clode and Marshall (2003b: 151) to observe nanocrystals (19 ± 0.8 to 400 nm in diameter) on the septal growth edge of *Galaxea fascicularis* that were interpreted as "basic elements of centers of calcification." In the same paper Clode and Marshall also observed nanometric components (21 ± 0.87 nm in diameter) within "fusiform crystals" developed on lateral flanks of septa (outside the zone of calcification centers). A breakthrough in understanding of the nanoscale relationships between the skeleton and polyp's soft tissue were images published by Clode and Marshall (2003a: figs. 1, 2). These authors observed randomly distributed nodular structures (23–48 nm in diameter: 37 ± 2nm average) on a mesh-like network of organic matrix at the calcifying interface penetrating between aragonite crystals and extending to calicoblastic cells. Although not emphasized by the authors, Clode and Marshall (2003 a: fig.1 reproduced herein as Fig. 15) were also the first who illustrated the entirely nanogranular internal structure of the skeletal fibers: nanograins ca. 50 nm in diameter are clearly distinguishable within larger, most likely acicular-type crystals. Stolarski (2003: 500) observed a twofold distribution of nanograins (ca. 50 nm in diameter) in polished, non-etched samples of azooxanthellate *Stephanocyathus paliferus* Cairns, 1977. In the organic-enriched RAF regions nanograins were dispersed, whereas in the bordering region of thickening fibers, the nanocomponents were not well seen. Subsequently, Cuif et al. (2004: 7) and Cuif and Dauphin (2005a, b) provided

clear-cut AFM evidence that the thickening fibers in *Merulina*, *Favia*, *Cladocora*, and *Caryophyllia* are composed entirely of nanograins (some tenths of nanometers in diameter) embedded in a thin layer of organic material. The organic material associated with nanograins was interpreted as mineralizing hydro-organic gel entrapped in the skeletal structure (Cuif and Dauphin 2005b).

AFM observations of calcium carbonate biocrystals from other invertebrate groups consistently show the occurrence of nanogranular components in: (1) calcite fibers of the spherulitic basal skeleton of a calcareous sponge, *Petrobiona* (nanograins ca. 50–100 nm in diameter, herein reported); (2) aragonite coenosteal fibers of the stylasteriid hydrozoan *Adelopora* (ca. 50–100 nm in diameter, herein reported); (3) aragonitic nacre layer of Recent and fossil cephalopods [nanograins 40–50 nm in diameter on average, in Recent (5–555 nm) and fossil (28–92 nm)], Dauphin 2001); (4) aragonitic nacre layer of the Recent bivalve *Pinctada* (nanograins ca. 45 nm in size surrounded by foam-like organic phase, Rousseau et al. 2005).

As noted here, nanograins (usually ca. 50 nm in diameter) seem to be a universal component of the calcareous biocrystals irrespective of taxonomic group or calcium carbonate polymorph. This uniform nanostructural pattern invites questions regarding biological vs. physicochemical factors controlling their formation. From the biological perspective, it would be tempting to relate the formation of nanograins directly to the physiological/biochemical processes that operate at the sub-cellular scale. Actually, two models of such biological mediation have been proposed that may also explain the nanometer size of the granular mineral components:

(1) Dimensions of the minute-scale skeletal components are constrained by "a dose" of mineralizing ions expelled by calicoblastic cells. For example, Isa (1986) regarded calcium-rich spherules found in sub-epithelial space of osmicated tissue from the scleractinian *Acropora hebes* as precursors of 50 nm aragonite granulae and sites of initial nucleation (vesicular exocytosis is regarded as due to artefacts by Clode and Marshall 2002);

(2) Dimensions of the minute-scale skeletal component correspond with the size of organic matrix compartments that serve as mineralization sites. For example, Wörheide et al. (1997: 1428) proposed that nanometric "seed crystals" of coralline sponge spherulites are formed within "small containers (30–50 nm)" of the three dimensional Ca^{2+} binding glycoproteic mucus organic network[3] in enlarged vacuoles of large vesicle cells (see also Reitner et al. 1997). Similar mechanisms were proposed by Clode and Marshall (2003a: 159) for scleractinians, suggesting that the "nascent $CaCO_3$ crystals may become established upon an organic matrix in distinct, isolated extracellular pockets". Interestingly, nanocomponents are visible in Clode and Marshall's (2003a) frozen hydrated sample (herein reproduced Fig. 15) and show twofold arrangement: (1) nodular structures (28–48 nm in diameter) interpreted as mineral components are dispersed within organic network (Fig. 15B), whereas (2) well defined biocrystals occurring just below the region of fibrilar matrix are composed of dense accumulations of slightly larger (ca. 50? nm) nanograins (Fig. 15A). One may assume that these two distinct regions of nanograin occurrence correspond to two distinct phases of skeleton formation: (1) nanograin formation on sulphur containing organic fibrillar matrix and (2) deposition of nanograins directly onto preformed crystals (Alan Marshall, personal communication 2005).

Clearly, additional experimental studies are needed prior to formulating a more comprehensive model of biologically-related interactions during nanograin formation and their aggregation. These studies may also give an insight into the physico-(bio)chemical properties (1st problem) and interactions (2nd problem) of inorganic and organic components that participate in nanograin formation that are highlighted below.

The first problem concerns the unknown original phase (amorphous [ACC] *versus* crystalline) of calcium carbonate nanograins *in statu nascendi*. As outlined clearly by Cohen and McConnaughey (2003: 158) it remains an open question "whether entire packets of crystalline aggregates are precipitated at once or whether individual amorphous granules are exocytosed into the subskeletal space, transported within their protein sheaths to the site of calcification and added one by one to a growing nuclear packet [...]". Although nanograins documented in some bacterial precipitates (e.g., López-Garcia et al. 2005) or aragonitic carbonate nodules deposited by scleractinian multicellular isolates (Domart-Coulon et al. 2001) showed purely crystalline character, it cannot be excluded that the mineral phase already (by the time of experiment) underwent phase transformation (ACC → crystalline $CaCO_3$), especially as ACC is a highly unstable form of calcium carbonate (see also Xu et al. 2005). As summarized in excellent fashion by Mann (2001: 62) "there is growing evidence that amorphous granules containing high levels of inorganic and organic components are prevalent in the early stages of many biomineralization systems. These structures are often formed away from the mineralization site and subsequently transported to the organic matrix where they aggregate in large numbers before undergoing phase transformation to more stable minerals." Indeed, amorphous precursors have been confirmed in calcitic biocrystals of sea urchin spines (Politi et al. 2004), calcium storage structures of some crustaceans (Raz et al. 2002; Becker et al. 2003), and molluscan larval shells (Weiss et al. 2002); see also Addadi et al. 2003; Weiner et al. 2003). Recently, Meibom et al. (2004: L23306) showed that Mg-enriched zones in scleractinian skeleton correlate with the beginning of fiber growth; since Mg is known as important stabilizing factor of ACC, they suggested that "high magnesium concentration might in part be the trace element signature of transient ACC [...]". Since the nanograins appear to be

[3] It remains to be investigated whether intra-vacuolar insoluble organic matrix is the original product of metabolism spherulite-forming large vesicle cells (LVC) or represents non-digested bacterial remains that are common in LVC acting as bacteriocytes (Wörheide 1998).

a component of a biocrystal in its entire length, then it remains to be answered whether only Mg-enriched zones were formed from the nanograins that underwent ACC → crystalline transformation (whereas nanograins from other parts of the fiber would have different formation history) or, that concentration of Mg in these regions is associated with organic components rather than with the mineral phase.

Still another problem awaiting explanation is the remarkably ordered structure of calcium carbonate fibers i.e., continuity of crystalographic axes within fibers despite their nanogranular structure. This crystallographic continuity clearly suggests that the nanograins are not randomly distributed but their aggregation into crystals is strictly organized. Such interactions during formation of coral fibers have been outlined by Cuif and Dauphin (2005b: 326) who suggested that the crystallographic continuity of fibers results from "some interactions [...] between fibre surfaces and the newly secreted mineralizing compounds at the beginning of a mineralization cycle, allowing the components of the polymer framework to be oriented according to the underlying fibers". Also, Rousseau et al. (2005) suggested that a single-crystal behavior of mollusk nacre tables (*Pinctada*), that are composed of coherent aggregation of crystalline nanograins (ca. 45 nm in size surrounded by foam-like organic phase), results from the heteroepithaxy of the intracrystalline organic matrix having crystalline structure.

Since the nanograins are also reported here from supposedly abiotically precipitated sparry calcite crystals, there is a need to consider factors other than biologically-related that may influence $CaCO_3$ nanograin precipitation. Our observations of nanostructures of sparry calcite recovered from the interseptal region of a Cretaceous calcitized scleractinian, shows that, although nanograins of similar sizes (ca. 60–100 nm) as those in biocrystals are recognizable, the roughness of the etched surface (z-scale max. 30 nm) is less than in biological samples (Fig. 12A); this suggests that the sparry calcite sample was less susceptible to oxidizing etching, hence it probably contained less intracrystalline organic material. Remarkably, sparry calcites recovered from the interseptal spaces of still aragonite coralla of the Triassic corals (Fig. 12B) did not exhibit nanograin structure even though subjugated to exactly the same preparatory procedures[4]. One may assume that, if the organized structure of the hydrogel organics is a prerequisite of nanograins formation then their presence (or, conversely, absence) from some sparry calcites implies the occurrence (or, conversely, a lack) of such organic components in their crystallization environment (see Fig. 16). This is supported by Kirkland et al. (1999: 349), who stated that rounded or anhedral ≤50 nm objects "are common in carbonates formed in organic-rich environments in nature." Because the material we examined was sparse, we were not able to analyze the possible organic content of the nanogranular sparry calcite, but this will be the next step in providing concluding arguments. The most suitable approach to investigate various factors controlling formation of the calcareous nanograin is by biomimetic studies. They hint that biochemical components present in mineralization site have a profound impact on the type of the mineral polymorph (e.g., Takahashi et al. 2005), shapes of crystals (e.g., Gower and Tirrell 1998; Naka and Chujo 2001), agglomeration behavior (e.g., Mann et al. 2000; Sayan 2005; Deng, et al. 2005), and other nanoscale phenomena (e.g., Astilleros et al. 2003).

Following this reasoning regarding organic mediation in nanograin formation, questions arise about the possible source of these components and about their properties: are these "specialized organic molecules" that derive directly from decomposition of the biomineralizing tissue of the organism (1), or are these components secreted by microorganisms active in mineral precipitation environment (2), or are they "generic" components of the so called Dissolved Organic Matter not directly linked with any organism but are present in the environment (3)? Remarkably, analogous questions concern researchers of calcareous nanoprecipitates (grains ca. 30–100 nm in diameter; see Kaźmierczak and Kempe 2003) formed in cyanobacteria-rich environments: is the nanograin formation controlled by these organisms directly (permineralization) or indirectly (secreted or cytolysis-derived organic components; see López-Garcia et al. 2005)? A comprehensive explanation of factors that influence nanograin formation will also be important in the astrobiological debate about the biotic *versus* abiotic interpretation of nanoscale structures recovered from some meteorites (like the celebrated Martian ALH84001 or Tataouine meteorite, see Benzerara et al. 2003).

Nanotaphonomy: preliminary remarks

An almost unexplored aspect of biominerals is their nanoscale behavior during diagenesis. In calcareous biocrystals examined here, the nanogranular structure faded only in skeletons that were prominently diagenetically altered i.e., partially calcitized Triassic *P. cylindrica*, whereas it was invariably present in Recent and fossil samples with the original mineral phase of the skeleton preserved. The taphonomic problem that emerges from this observation is whether the nanogranular structure of fibers can be used as a proxy of pristine preservation or do the nanograins also occur in diagenetically altered skeletons if certain physicochemical conditions are fulfilled? We have approached this problem first by comparing some overall biogeochemical parameters of the skeleton in the Triassic *P. cylindrica* (without nanograins), and in corals whose skeletal fibers have well developed nanogranular structure

[4] Research at the nanoscale require particularly rigorous protocols to be used to avoid e.g., preparative artifacts. For example, Kirkland et al. (1999: figs. 6-8) showed that nanograin objects ca. 70 nm in diameter may appear on euhedral rhombic calcite crystals as a result of acidic etching. A support that the reported herein nanograins are not preparative artifacts provides lack of any textural response of synthetically and sterile produced aragonite crystals on the use of oxidizing solution (exactly the same protocol as for other examined samples).

(Recent *F. stelligera*, Cretaceous *R. complanata*, Jurassic *I.* cf. *bernensis*, and the Triassic tropiastraeid).

Mineral phase.—Since Magnesium (Mg) fits well into calcite lattice and Strontium (Sr) fits well into aragonite one, the proportions of both elements in the sample are commonly used as a proxy of biogenic aragonite-calcite transformation (e.g., Scherer 1977; Brand 1989; see also overview Sorauf and Cuif 2001). Partial calcitized fibrous wall of *P. cylindrica* shows the highest Mg and lowest Sr levels in bulk analysis. The WDS mapping indicates spotted distribution of Mg-enriched (calcitized) regions; mid-septal zone is completely replaced with calcite as supported by homogenous Mg distribution and by staining with Feigl's solution. Conversely, a high level of Sr and a low one of Mg was a feature of fibrous skeletal part of all corals with aragonite mineralogy, though differences in Mg and Sr distribution in comparison to Recent corals, hint at possibly different taphonomic pathways. Fibers of extant *F. stelligera*, in comparison to fossil aragonite coralla (except of *I.* cf. *bernensis*) contains relatively high amount of Sr and, respectively low amount of Mg. Slightly higher concentration of Mg (depletion in Sr) that can be observed along the mid-septal zone may be congruent with observation by Meibom et al. (2004) that Mg-enriched zones occur in "centers of calcification" and at the beginning of the biomineralization step within fibers, as a possible signature of original amorphous phase. Although the mid-septal zone of *R. complanata* skeleton is also Mg-enriched (and Sr-depleted), the signal is stronger than in *F. stelligera* and possibly, as suggested by Sorauf (1999: 1037) who examined the same specimen, is related to early diagenetic calcitization of this zone (we have not proved this as our XRD analyses concerned fibers, and staining with Feigl's solutions were inconclusive). Calcification centers in *I.* cf. *bernensis* and the Triassic tropiastraeid are not easily discernible on Sr and Mg WDS maps, possibly suggesting obliteration of the original signal by secondary aragonite-to-aragonite recrystallization (e.g., Perrin 2004: 95). Additional argument that the mineral phase of our Triassic tropiastraeid has been diagenetically altered is its enrichment with respect to Sr and strong depletion with respect to Mg (that would balance Sr enrichment).

Organic phase.—A simple method to assess occurrence of organic matter concentrations is to observe chromatic response of acridine orange-stained samples under fluorescent microscope (Gautret et al. 2000; Stolarski 2003): the most prominent chromatic response exhibits organic matter concentrated in centers of calcification, whereas typically much weaker response shows the organic matter concentrated along the thickening fibers' growth steps (see Stolarski 2003: fig. 11C). Chromatic response of the highly dispersed organic components associated with the skeletal nanograins (Cuif et al. 2004; Cuif and Dauphin 2005a, b) cannot be unambiguously detected by this method, but probably contributes to the background response of the sample. The lack of distinct chromatic response of the calcification centers and other skeletal regions of the examined herein fossil coralla in comparison to Recent samples, suggests that the bulk of the intraskeletal organic matter has been decomposed and removed from the skeleton. This is consistent with observations that decomposition of intraskeletal organic phase starts immediately after skeleton formation (this can be quantified by the amino acid recemization ratio in the historical time scale e.g., Mitterer 1993, Nyberg et al. 2001, or, in the geological time scale, by the changed proportions in amino acid composition Gautret and Marin 1993). Consequently, coralla of fossil scleractinians often contain only few percent of supposed original organic content (Cuif et al. 1992), nonetheless some researchers extracted significantly more organic components from the fossil coralla (e.g., Muscatine et al. 2005 estimated organic content of the Triassic *Pachythecalis* for ca. 1.19% of skeleton weight, almost equal to the amount known extracted from Recent coralla i.e., 0.01–1.5% of skeleton weight).

Although the bulk of the organic components has been removed from calcification centers of examined fossil corals, their occurrence within fibers and their stabilizing role in nanograin preservation is indirectly supported by a distinct etching relief of samples submerged in oxidizing solution (recently we have also isolated various aminoacids from these skeletons but quantitative data require verification and will be publish elsewhere; Stolarski unpublished data). Thermogravimetric analysis was another, indirect method to attest presence of the organic content within fibrous skeleton and its association with nanograins. A distict weight loss on thermogravimetrical curve reported for *F. stelligera* (about 1.5%) and *I.* cf. *bernensis* (about 1.8%) suggests occurrence of nanograin-associated hydrated organic matter. Additional support for the organic composition of the removed components provides a distinct (in *F. stelligera*) exotherm elevation on the differential thermo-analytical curve that follows endotherm peak, most likely resulting from a rapid oxidization of the organic phase. Conversely, lack of nanogranular texture in partially calcitized skeleton of the Triassic *P. cylindrica* correlates with significantly depleted amount of supposedly organic phase (about 0.76% weight loss) in comparison to Recent and Jurassic samples. The above results support the hypothesis by Cuif et al. (2004) and Cuif and Dauphin (2005a, b) about the organic nature of the strongly interactive material associated with nanograins. In conclusion (Fig. 16), we assume that organic phase materials trapped within the skeleton (the remnants of the original hydro-organic gel, a medium of nanograin formation) is the main stabilizing factor that aids preservation of nanocomponents in fibers of Recent and fossil corals. The removal of organic components from the skeleton during diagenesis e.g., by phase transformation of the aragonite to calcite, usually results in loss of the original nanogranular structure. It is also possible that weaker etching relief in some regions of fibrous skeleton (described herein as "floe" textures; Figs. 6–8) may be connected with depleted amount of organic components.

Diagenetic changes that affect the skeletal mineral phase, if not coupled with organic phase removal, seem to exert no

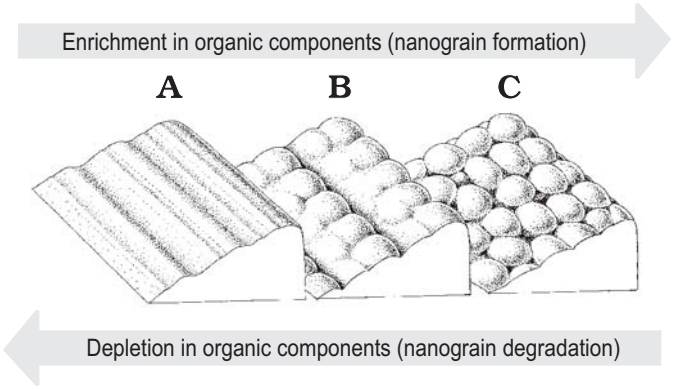

Fig. 16. Main nanostructural patterns of calcium carbonate crystals and their possible diagenetic pathways. Nanostructural spectrum encompasses: crystals without nanograins (**A**, based on synthetically produced $CaCO_3$ crystals, Fig. 1); crystals composed entirely of nanograins (**C**, based on Recent biocrystals formed in hydro-organic gel); and crystals with intermediate nanostructural pattern, having a bumpy texture representing degraded/fused nanograins (**B**, based on *P. cylindrica* skeleton, Fig. 11).

influence on preservation of nanogranular structure of the biomineral. If our interpretation regarding the influence of organic components on formation of nanograins in some sparry calcites is supported, then it can be expected that in certain diagenetic regimes (with the presence of organic hydrogel) aragonite → calcite recrystallization may result in the formation of nanograins that will clearly have a secondary origin.

Conclusions

- Biocrystals with an aragonite mineral phase that form the fibrous skeleton of Recent scleractinians (*Favia*, *Goniastraea*), stylasterid coenosteum (*Adelopora*), and calcite fibers of the basal skeleton of the calcareous sponge (*Petrobiona*), consist entirely of grains ca. 50–100 nm in diameter separated from each other by spaces of a few nanometers.
- Also skeletal fibers of the fossils scleractinians (Neogene *Paracyathus*, Cretaceous *Rennensismilia*, and *Trochocyathus*, Jurassic *Isastraea*, and Triassic unidentified tropidastraeid), whose mineral phase is aragonitic, have nanogranular structure (grains ca. 50–100 nm). Conversely, nanograins have not been recognized within partly calcitized fibers of the Triassic coral (*Pachysolenia*), most samples of sparry calcite, nor in synthetic aragonite crystals prepared in sterile environment.
- Distinctly granular *versus* "bumpy" (without distinct nanograins as in *Pachysolenia*) patterns of nano-organization of $CaCO_3$ biocrystals seem to correspond, respectively, to "normal" *versus* diagenetically depleted amounts of organic matter contained within the mineral phase.
- Occurrence of nanograins in crystals of some sparry calcite (Lubycza Królewska locality) regarded as abiotically precipitated suggests that nanogranular organization of calcium carbonate fibers is not evidence *per se* of their biogenic *versus* abiogenic origin or their aragonitic *versus* calcitic composition, but rather seems to be a feature of $CaCO_3$ formed in an aqueous solution in the presence of molecules controlling nanograin formation (hydro-organic gel).

Glossary

The glossary provides brief definitions of terminology used in this paper.

Amorphous – non-crystalline
Biocrystal – crystal grown in a biological environment (e.g., in living organism)
Crystal – monocrystal or polycrystal
Crystalline – monocrystalline or polycrystalline
Crystallite – nanometer-sized monocrystalline region of a polycrystal
Fiber – a slender and greatly elongated object, in particular → biocrystal.
Monocrystal (single crystal) – any solid material in which an orderly three-dimensional definite arrangement of the atoms, ions or molecules is repeated throughout the entire volume.
Monocrystalline – made of a monocrystal
Nanograin, **nanogranule** – nanometer-sized particle (crystalline or amorphous)
Polycrystal – any solid material composed of randomly oriented or ordered monocrystalline regions.
Polycrystalline – made of a polycrystal

Acknowledgements

We have benefited a lot from helpful comments by reviewers of this paper: Jean-Pierre Cuif (Université Paris-Sud XI, Orsay, France) and Jim Sorauf (Binghamton University, USA). Jim Sorauf and Steve Cairns (The National Museum of Natural History, Washington, D.C.) corrected the language of this paper. We are grateful to Ann Budd, Jean-Pierre Cuif, Antonio Russo (Università di Modena e Reggio Emilia, Modena, Italy), and Helmut Zibrowius (Station marine d'Endoume, Marseille, France) who generously provided Recent (A.B., H.Z.) and fossil (J.-P.C., A.R.) specimens. Many thanks are due to Piotr Dzierżanowski (Faculty of Geology, Warsaw University, Poland) and Michał Kuźniarski (Institute of Geological Sciences, Warsaw, Poland) who kindly helped us to gather geochemical analyses of samples. Alan Marshall (La Trobe University, Melbourne, Australia) provided useful comments and together with Peta Clode (The University of Western Australia, Crawley) gave permission to use published photographic materials in composition of Fig. 15 in this paper. This work was partly supported by financial sponsorship provided by Italian Ministry of University and Scientific and Technological Research Grant MURST (project Cofin 2002). This is the first publication of the BIOMIMAT (Biominerals, Biomimetics, Biomaterials) initiative, which aims to stimulate interdisciplinary research on origin, evolution, formation, and practical applications of biominerals.

References

Addadi, L., Raz, S., and Weiner, S. 2003. Taking advantage of disorder: amorphous calcium carbonate and its roles in biomineralization. *Advanced Materials* 15: 959–970.

Astilleros, J.M., Pina, C.M., Fernández-Díaz, and Putnis, A. 2003. Nanoscale growth of solid crystallising from multicomponent aqueous solutions. *Surface Science* 545: L767–L773.

Barnes, D.J. 1970. Coral skeletons: an explanation of their growth and structure. *Science* 170: 1305–1308.

Becker, A., Bismayer, U., Epple, M., Fabritius, H., Hasse, B., Shi, J., and Ziegler, A. 2003. Structural characterisation of X-ray amorphous calcium carbonate (ACC) in sternal deposits of the crustacea *Porcellio scaber*. *Dalton Transactions* 2003: 551–555.

Benzerara, K., Menguy, N., Guyot, F., Dominici, C., and Gillet, P. 2003. Nanobacteria-like calcite single crystals at the surface of the Tataouine meteorite. *Proceedings of the National Academy of Sciences* 100: 7438–7442.

Brand, U. 1989. Aragonite-calcite transformation based on Pennsylvanian molluscs. *Geological Society of America Bulletin* 101: 377–390.

Bryan, W. H. and Hill, D. 1942. Spherulitic crystallization as a mechanism of skeletal growth in the Hexacorals. *Proceedings of the Royal Society of Queensland* 52: 78–91.

Cairns, S.D. 1977. A revision of the recent species of *Stephanocyathus* (Anthozoa: Scleractinia) in the western Atlantic, with descriptions of two new species. *Bulletin of Marine Science* 27: 729–739.

Cairns, S.D. 1991. The marine fauna of New Zealand: Stylasteridae (Cnidaria: Hydroida). *New Zealand Oceanographic Institute Memoir* 98: 1–180.

Cairns, S.D., Hoeksema, B.W., and Van Der Land, J. 1999. Appendix: List of Stony Coral. *In*: S.D. Cairns, Species Richness of Recent Scleratinia. *Atoll Research Bulletin* 459: 13–16.

Cieśliński, S. and Rzechowski, J. 1993. Mapa geologiczna podłoża czwartorzędu Roztocza między Tomaszowem Lubelskim a Hrebennem. *In*: M. Harasimiuk, J. Krawczuk, and J. Rzechowski (eds.), *Tektonika Roztocza i jej aspekty sedymentologiczne, hydrologiczne i geomorfologiczno-krajobrazowe*, 38–46. Towarzystwo Wolnej Wszechnicy Polskiej, Lublin.

Clode, P.T. and Marshall, A.T. 2002. Low temperature FESEM of the calcifying interface of a scleractinian coral. *Tissue and Cell* 34: 187–198.

Clode, P.L. and Marshall, A.T. 2003a. Calcium associated with a fibrillar organic matrix in the scleractinian coral *Galaxea fascicularis*. *Protoplasma* 220: 153–161.

Clode, P.L. and Marshall, A.T. 2003b. Skeletal microstructure of *Galaxea fascicularis* exsert septa: a high-resolution SEM study. *Biological Bulletin* 204: 146–154.

Cohen, A.L. and McConnaughey, T.A. 2003. Geochemical perspectives on coral mineralization. *In*: P.M. Dove, J.J. De Yoreo, and S. Weiner (eds.), Biomineralization. *Reviews in Mineralogy and Geochemistry* 54: 151–185.

Constantz, B.R. 1986a. Coral skeleton construction: a physiochemically dominated process. *Palaios* 1: 152–157.

Constantz, B.R. 1986b. The primary surface area of corals and variations in their susceptibility to diagenesis. *In*: J.H. Schroeder and B.H. Purser (eds.), *Reef Diagenesis*, 53–76. Springer-Verlag, Berlin.

Cuif, J.P. 1975. Caracteres morphologiques, microstructuraux et systematiques des Pachythecalidae, nouvelle famille de Madreporaires triasiques. *Geobios* 8: 157–180.

Cuif, J.-P. and Dauphin, Y. 1998. Microstructural and physico-chemical characterization of "centers of calcification" in septa of some Recent scleractinian corals. *Paläontologische Zeitschrift* 72: 257–270.

Cuif, J.-P. and Dauphin, Y. 2005a. The environment recording unit in coral skeletons—a synthesis of structural and chemical evidences for a biochemically driven, stepping-growth process in fibers. *Biogeosciences* 2: 61–73.

Cuif, J.-P. and Dauphin, Y. 2005b. The two-step mode of growth in the scleractinian coral skeletons from the micrometre to the overall scale. *Journal of Structural Biology* 150: 319–331.

Cuif, J.-P. and Sorauf, J.E. 2001. Biomineralization and diagenesis in Scleractinia: part I, biomineralization. *Bulletin of the Tohoku University Museum* 1: 144–151.

Cuif, J.-P., Dauphin, Y., and Gautret, P. 1997. Biomineralization features in scleractinian coral skeletons: source of new taxonomic criteria. *Boletín de la Real Sociedad Española de Historia Natural (Sección Geológica)* 92: 129–141.

Cuif, J.-P., Dauphin, Y., Doucet, J., Salome, M., and Susini, J. 2003. XANES mapping of organic sulfate in three scleractinian coral skeletons. *Geochimica et Cosmochimica Acta* 67: 75–83.

Cuif, J.-P., Dauphin, Y. Berthet, P., and Jegoudez, J. 2004. Associated water and organic compounds in coral skeletons: Quantitative thermogravimetry coupled to infrared absorption spectrometry. *Geochemistry, Geophysics, Geosystems* 5: Q11011, doi:10.1029/2004GC000783.

Cuif, J.-P., Dauphin, Y., Freiwald, A. Gautret, P., and Zibrowius, H. 1999. Biochemical markers of zooxanthellae symbiosis in soluble matrices of skeleton of 24 Scleractinia species. *Comparative Biochemistry and Physiology A* 123: 269–278.

Cuif, J.-P., Fischer, J.-C., and Marcoux, J. 1972. Découverte d'une faune de Chaetetida dans le Trias supérieur de Turquie. *Comptes rendus hébdomadaires des séances de l'Académie des Sciences D* 275: 185–188.

Cuif, J.-P., Lecointre, G., Perrin, C., Tillier, A., and Tillier, S. 2003. Patterns of septal biomineralization in Scleractinia compared with their 28S rRNA phylogeny: a dual approach for a new taxonomic framework. *Zoologica Scripta* 32: 459–473.

Dana, J.D. 1846. Zoophytes. *United States exploring expedition during the years 1838–1842, under the command of Charles Wilkes* 7: 1–740.

Dauphin, Y. 2001. Nanostructures de la nacre des tests de céphalopodes actuels. *Paläontologische Zeitschrift* 75: 113–122.

Dauphin, Y. 2002. Fossil organic matrices of the Callovian aragonitic ammonites from Lukow (Poland): location and composition. *International Journal of Earth Sciences (Geologische Rundschau)* 91: 1071–1080.

Deng, S.G., Cao, J.M., Feng, J. Guo, J. Fang, B.Q., Zheng, M.B., and Tao, J. 2005. A bio-inspired approach to the synthesis of $CaCO_3$ spherical assemblies in a soluble ternary-additive system. *Journal of Physical Chemistry B* 109: 11473–11477.

Domart-Coulon, I.J., Elbert, D.C., Scully, E.P. Calimlim, P.S., and Ostrander, G.K. 2001. Aragonite crystallization in primary cell cultures of multicellular isolates from a hard coral. *Pocillopora damicornis*. *Proceedings of the National Academy of Sciences* 98: 11885–11890.

Felix, J. 1903. Die Anthozoen der Gosauschichten in den Ostalpen. *Palaeontographica* 49: 163–359.

Friedman, G.M. 1959. Identification of carbonate minerals by staining methods. *Journal of Sedimentary Petrology* 29: 87–97.

Gautret, P. and Marin, F. 1993. Evaluation of diagenesis in scleractinan corals and calcified demosponges by substitution index measurement and intraskeletal organic matrix analysis. *Courier Forschungsinstitut Senckenberg* 164: 317–327.

Gautret, P., Cuif, J.-P., and Stolarski, J. 2000. Organic components of the skeleton of scleractinian corals – evidence from in situ acridine orange staining. *Acta Palaeontologica Polonica* 45: 107–118.

Geist, J., Auerswald, K., and Boom, A. 2005. Stable carbon isotopes in freshwater mussel shalls: Environmental record or marker for metabolic activity? *Geochimica et Cosmochimica Acta* 69: 3545–3554.

Goldfuss, A. 1926. *Petrefacta Germaniae*. 252 pp. Arnz, Düsseldorf.

Gower, L.A. and Tirrell, D.A. 1998. Calcium carbonate films and helices grown in solution of poly(aspartate). *Journal of Crystal Growth* 191: 153–160.

Isa, Y. 1986. An electron microscope study on the mineralization of the skeleton of the staghorn coral *Acropora hebes*. *Marine Biology* 93: 91–101.

Johnston, I.S. 1980. The ultrastructure of skeletogenesis in hermatypic corals. *International Review of Cytology* 67: 171–214.

Kirkland, B.L., Lynch, F.L., Rahnis, M.A., Folk, R.L., Molineux, I.J., and McLean, R.J.C. 1999. Alternative origins for nannobacteria-like objects in calcite. *Geology* 27: 347–350.

Kaźmierczak, J. and Kempe, S. 2003. Modern terrestrial analogues for the carbonate globules in Martian meteorite ALH84001. *Naturwissenschaften* 90: 167–172.

Lamarck, J.B. 1816. *Histoire naturelle des animaux sans vertebres. Tome 2*. 568 pp. Verdiere, Paris.

Linnaeus, C. 1767. *Systema naturae, sive Regna tria Naturae systematice proposita per classes, ordines, genera et species* 1 (2) 12 edition, 533–1327. Laurentius Salvius, Stockholm.

López-Garcia, P., Kaźmierczak, J., Benzerara, K., Kempe, S. Guyot, F., and Moreira, D. 2005. Bacterial diversity and carbonate precipitation in the giant microbialites from the highly alkaline Lake Van, Turkey. *Extremophiles* 9: 263–274.

Mann, S. 2000. Crystal tectonics: Chemical construction and self-organiza-

tion beyond the unit cell. *Journal of the Royal Chemical Society, Dalton Transactions* 2000: 3753–3763.

Mann, S. 2001. *Biomineralization: Principles and Concepts in Bioinorganic Materials Chemistry*. 216 pp. Oxford University Press, Oxford.

Marin, F. and Luquet, G. 2004. Molluscan shell proteins. *Comptes Rendus Palevol* 3: 469–492.

Meibom, A., Cuif, J.-P., Hillion, F., Constantz, B. R., Juillet-Leclerc, A., Dauphin, Y., Watanabe, T., and Dunbar, R.B. 2004. Distribution of magnesium in coral skeleton. *Geophysical Research Letters* 31: doi: 10.1029/2004GL021313.

Mitterer, R.M. 1993. The diagenesis of proteins and amino acids in fossil shells. *In*: M.H. Engel and S.A. Macko (eds.), *Organic Geochemistry*, 739–753. Plenum Press, New York.

Muscatine, L., Goiran, C. Land, L. Jaubert, J. Cuif, J-P, and Allemand, D. 2005. Stable isotopes ($\delta^{13}C$ and $\delta^{15}N$) of organic matrix from coral skeleton. *Proceedings of the National Academy of Sciences* 102: 1525–1530.

Naka, K. and Chujo, Y. 2001. Control of crystal nucleation and growth of calcium carbonate by synthetic substrates. *Chemical Materials* 13: 3245–3259.

Nyberg, J., Csapo, J., Malmgren, B., and Winter, A. 2001. Changes in the D- and L-content of aspartic acid, glutamic acid, and alanine in a scleractinian coral over the last 300 years. *Organic Geochemistry* 32: 623–632.

Perrin, C. 2004. Early diagenesis of carbonate biocrystals : isomineralogical changes in aragonite coral skeletons. *Bulletin de la Société Géologique de France* 175: 95–106.

Philippi, R.A. 1842. Zoologische Beobachtungen. 6. Verzeichniss der im Mittelmeer von mir beobachteten Arten *Cyathina* Ehrenberg. *Archiv für Naturgeschichte* 8: 40–44.

Politi, Y. Arad, T., Klein, E., Weiner, S., and Addadi, L. 2004. Sea urchin spine calcite forms via a transient amorphous calcium carbonate phase. *Science* 306: 1161–1164.

Raz, S., Testeniere, O. Hecker, A. Weiner, S., and Luquet, G. 2002. Stable amorphous calcium carbonate is the main component of the calcium storage structures of the crustacean Orchestia cavimana. *Biological Bulletin* 203: 269–274.

Reitner, J. 1992. "Coralline Spongien" – Der Versuch einer phylogenetisch-taxonomischen Analyse. *Berliner Geowissenschaftliche Abhandlungen E* 1: 1–352.

Reitner, J., Wörheide, G., Lange, R., and Thiel, V. 1997. Biomineralization of calcified skeletons in three Pacific coralline demosponges—an approach to the evolution of basal skeletons. *Courier Forschungs-Institut Senckenberg* 201: 371–383.

Reuss, A.E. 1871. Die fossilen Korallen des österreichisch-ungarischen Miozäns. *Denkschriften der Kaiserlichen Akademie der Wissenschaften, Mathematisch-naturwissenschaftliche Classe* 31: 197–270.

Rousseau, M., Lopez, E., Stempflé, P., Brendlé, M., Franke, L., Guette, A., Naslain, R., and Bourrat, X. 2005. Multiscale structure of sheet nacre. *Biomaterials* 26: 6254–6262.

Roniewicz, E. 1982. Pennular and non-pennular Jurassic scleractinians—some examples. *Acta Palaeontologica Polonica* 24: 157–193.

Roniewicz, E. 1984. Aragonitic Jurassic corals from erratic boulders on the South Baltic coasts. *Annales Societatis Geologorum Poloniae* 54: 65–77.

Sayan, P. 2005. Effect of sodium oleate on the agglomeration of calcium carbonate. *Crystal Research and Technology* 40: 226–232.

Sinclair, D.J. 2005. Correlated trace element "vital effects" in tropical corals: A new geochemical tool for probing biomineralization. *Geochimica et Cosmochimica Acta* 69: 3265–3284.

Scherer, M. 1977. Preservation, alternation and multiple cementation of aragonitic skeletons from the Cassian Beds (U. Triassic, Southern Alps): petrographic and geochemical evidence. *Neues Jahrbuch für Geologie und Paläontologie – Abhandlungen* 154: 213–262.

Sorauf, J.E. 1999. Skeletal microstructure, geochemistry and organic remnants in Cretaceous scleractinian corals: Santonian Gosau Beds of Gosau, Austria. *Journal of Paleontology* 73: 1029–1041.

Sorauf, J.E. and Cuif, J.-P. 2001. Biomineralization and diagenesis in Scleractinia: part II, diagenesis. *Bulletin of the Tohoku University Museum* 1: 152–163.

Stolarski, J. 1991. Miocene Scleractinia from Holy Cross Mountains , Poland; Part 1. Caryophylliidae, Flabellidae, Dendrophylliidae and Micrabaciidae. *Acta Geologica Polonica* 41: 37–67.

Stolarski, J. 2003. Three-dimensional micro- and nanostructural characteristics of the scleractinian coral skeleton: A biocalcification proxy. *Acta Palaeontologica Polonica* 48: 497–530.

Takahashi, K. Kobayashi, A. Doi, M. Adachi, S., Taguchi, T., Okamura, T. Yamamoto, H., and Ueyama, N. 2005. Restriction of $CaCO_3$ polymorh by NH···O hydrogen-bonded poly(methacryloylaminocarboxylate) ligands: induced polymorh change by strength and/or formation manner of hydrogen bond. *Journal of Materials Chemistry* 15: 2178–2187.

Thurmann, J. and Étallon, A. 1864. Lethea Bruntrutana, ou études paléontologiques et stratigraphiques sur le Jura Bernois et en particulier les environs de Porrentruy. *Neue Denkschriften der allgemeinen Schweizerischen Gesellschaft für die gesammten Naturwissenschaften* 20: 357–412.

Towe, K.M. 1972. Invertebrate shell structure and the organic matrix concept. *Biomineralization* 4: 1–14.

Wainwright, S.A. 1964. Studies of the mineral phase of coral skeleton. *Experimental Cell Research* 34: 213–230.

Watanabe, T., Fukuda, I., China, K., and Isa, Y. 2003. Molecular analyses of protein components of the organic matrix in the exoskeleton of two scleractinian coral species. *Comparative Biochemistry and Physiology B* 136: 767–774.

Weiner, S., Levi-Kalisman, Y, Raz, S., and Addadi, L. 2003. Biologically formed amorphous calcium carbonate. *Connective Tissue Research* 44: 214–218.

Weiss, I.M., Tuross, N., Addadi, L., and Weiner, S. 2002. Mollusc larval shell formation: amorphous calcium carbonate is a precursor phase for aragonite. *Journal of Experimental Zoology* 293: 478–491.

Wells, J.W. 1933. Corals of the Cretaceous of the Atlantic and Gulf Costal Plains and W-Interior of the United States. *Bulletins of American Paleontology* 18: 83–292.

White, C.A. 1879. Contribution to paleontology No. 1: Cretaceous fossils of the western states and territories. *Annual Report of the United States geological and geographical Survey of the Territories* 11 (for 1877): 273–319.

Wörheide, G. 1998. The reef cave dwelling ultraconservative coralline demosponge *Astrosclera willeyana* Lister 1900 from the Indo-Pacific. *Facies* 38: 1–88.

Vacelet, J. and Lévi, C. 1958. Un cas de survivance en Méditerranée, du grupe d'éponges fossiles des Pharétronides. *Comptes rendus hebdomadaires des séances de l'Académie des sciences* 246: 318–320.

Volz, W. 1896. Die Korallenfauna der Trias. II. Die Korallen der Schichten von St. Cassian in Süd Tirol. *Palaeontographica* 43: 1–124.

Xu, X., Han, J.T, and Cho, K. 2005. Deposition of amorphous calcium carbonate hemispheres on substrates. *Langmuir* 21: 4801–4804.